A high-order conservative positivity-preserving discontinuous Galerkin method for radiative transfer equations with diffusion synthetic acceleration

Xiaolu Gu[1], Juan Cheng[2], Dan Ling[3] and Chi-Wang Shu[4]

Abstract

This work develops a high-order conservative positivity-preserving discontinuous Galerkin (DG) method for the radiative transfer equation (RTE), integrated with a diffusion synthetic acceleration (DSA) strategy. The strategy is designed to address the slow convergence of source iteration in optically thick and highly scattering regimes, as well as the occurrence of negative radiation intensity values that may arise in high-order discretizations. The method employs a high-order DG spatial discretization and constructs a DSA operator through the asymptotic analysis of the discrete-ordinate formulation of the RTE. The moment-based P_1 update procedure, extended from linear to high-order DG discretizations, incorporates the diffusion correction into the high-order DG transport unknowns, ensuring both stability and effective acceleration. To guarantee physical admissibility, a positivity-preserving procedure based on locally conservative quantities is introduced, preserving non-negativity while maintaining conservation and high-order accuracy in the DG solution. The resulting algorithm significantly improves convergence speed, retains high-order accuracy, and produces non-negative radiation intensities in the final numerical solution. Numerical results for both one- and two-dimensional problems demonstrate the accuracy, efficiency, and robustness of the proposed method.

Keywords: Radiative transfer equation, Discontinuous Galerkin method, High-order accuracy, Positivity-preserving, Conservative schemes, Diffusion synthetic acceleration

[1]School of Mathematics and Statistics, Zhengzhou University, Zhengzhou, Henan 450001, China. E-mail: xlgu@zzu.edu.cn. The work of this author was partially supported by Youth Foundation of National Key Laboratory of Computational Physics (Grant No. 6142A05QN250312).

[2]Corresponding author. Academy for Multidisciplinary Studies, Capital Normal University, Beijing 100048, China. E-mail: jcheng@cnu.edu.cn. The work of this author was partially supported by NSFC grant 12571432 and National Key R&D Program of China No. 2023YFA1009003.

[3]School of Mathematics and Statistics, Xi'an Jiaotong University, Xi'an, Shaanxi 710049, China. E-mail: danling@xjtu.edu.cn. The work of this author was partially supported by NSFC grant 12101486 and Fundamental Research Funds for the Central Universities (Grant No. xxj032025062).

[4]Division of Applied Mathematics, Brown University, Providence, RI 02912. E-mail: chi-wang_shu@brown.edu. The work of this author was partially supported by NSF grant DMS-2309249.

1 Introduction

The radiative transfer equation models the propagation of radiation through a participating medium in the presence of scattering, absorption, and emission, and arises in a broad range of scientific and engineering applications, including astrophysics, optical imaging, shielding, and atmospheric and space radiation transport. From a mathematical standpoint, the RTE is a high-dimensional integro-differential equation whose solution depends on spatial, angular, temporal, and energetic variables. The high dimensionality together with the strong coupling induced by scattering interactions renders analytical solutions generally unavailable and poses substantial challenges for numerical computation, particularly in terms of accuracy, robustness, and computational efficiency.

A variety of numerical techniques have been developed for the radiative transfer equation, including Monte Carlo methods [6, 7], discrete-ordinate methods [4, 15], spherical harmonics methods [19], spectral methods [10], finite difference methods [29], finite volume methods [20], and finite element methods [21]. Among these approaches, the discrete-ordinate method (S_N) has been widely adopted due to its accuracy, flexibility, and relatively moderate computational cost. In the S_N formulation, the angular dependence of the radiation intensity is approximated by a finite set of discrete directions associated with a quadrature rule. This angular discretization transforms the radiative transfer equation into a system of linear hyperbolic transport equations posed in the physical space, in which the directional components are coupled through the scattering source terms.

In the numerical solution of radiative transfer equations within S_N formulations, discontinuous Galerkin methods have become a widely used spatial discretization approach. Since their introduction for neutron transport problems [22], DG methods have been extensively developed and applied to a broad class of convection-dominated equations [5]. They possess a number of attractive properties, such as high-order accuracy, geometric flexibility, suitability for h- and p-adaptivity, and a highly local data structure. These features lead to high parallel efficiency and are supported by a solid theoretical foundation for stability and error

analysis. Owing to these advantages, DG discretizations have been successfully employed in S_N radiative transfer calculations [17, 23, 32] and they constitute the spatial discretization framework adopted in the present work.

In S_N formulations combined with spatial discretizations such as DG methods, the angular discretization couples the resulting transport equations through the scattering source terms, leading to large scale algebraic systems that are difficult to solve efficiently. A commonly adopted approach to handle this coupling is source iteration (SI) [16], in which the scattering source is updated iteratively based on the previous solution. Although SI is simple to implement and effective in optically thin regimes, its convergence degrades severely in optically thick and strongly scattering media. In such regimes, the associated iteration operator has a spectral radius close to unity, resulting in very slow residue reduction and, in extreme cases, false convergence [1]. These limitations significantly restrict the efficiency of SI for scattering-dominated radiative transfer equations and highlight the necessity of incorporating effective acceleration techniques.

To alleviate the slow convergence of source iteration in scattering-dominated regimes, diffusion synthetic acceleration has been developed as one of the most effective and widely used acceleration techniques for discrete-ordinate radiative transfer equations [1, 2, 11]. The basic idea of DSA is to augment the transport iteration with an auxiliary diffusion equation, which acts as a preconditioner and significantly improves convergence in optically thick and highly scattering media. A fundamental requirement for the robustness and stability of DSA is the discrete consistency between the diffusion operator and the underlying transport discretization. In particular, the spatial discretization of the diffusion equation must reflect the asymptotic diffusion behavior of the discretized transport operator, so that the accelerated iteration remains stable and effective in the diffusive limit [1,11]. For DG methods of the S_N transport equation, considerable effort has been devoted to constructing diffusion operators that are compatible with the DG transport scheme. Fully consistent DSA approaches based on stabilized discretizations of the first-order spherical-harmonics (P_1) equations were devel-

oped for DG transport schemes [27, 28]. High-order DG S_N transport discretizations have also been accelerated using diffusion-based techniques. Representative examples include the interior-penalty based DSA formulations [24] and diffusion based preconditioning techniques developed for DG transport schemes on high-order curved meshes [9]. In addition to the construction of compatible diffusion operators, another aspect that has been explored concerns how diffusion corrections are incorporated into the transport solution. Early work by Wareing [25] proposed a moment-based update procedure for linear DG transport schemes, in which the diffusion correction is reconstructed using low-order angular moment information derived from the transport error equation. While this approach provides a practical mechanism for incorporating diffusion corrections into the DG transport solution, its extension to high-order DG schemes has not been explicitly addressed in the literature.

In addition to solver efficiency, maintaining the non-negativity of the radiation intensity is essential for the physical reliability of numerical solutions to the radiative transfer equation. The radiation intensity represents the radiative energy transported per unit time and per unit solid angle, and negative values are physically inadmissible. In practical computations, however, spurious oscillations may arise, particularly when high-order spatial discretizations are employed, leading to the appearance of negative intensities. Such nonphysical solutions not only violate fundamental physical principles but may also degrade numerical stability and adversely affect the convergence of iterative solvers. Consequently, the enforcement of non-negativity constitutes a fundamental requirement in the design of robust numerical methods for radiative transfer problems. A variety of positivity-preserving approaches have been proposed in the literature to address this issue, including characteristic-based schemes [13,14], exponential or non-polynomial discretizations [26], and nonlinear moment-preserving corrections to linear discontinuous Galerkin formulations [18]. While these methods can prevent the occurrence of negative intensities, they are often limited by low-order accuracy, reliance on characteristic tracing, nonlinear procedures requiring additional local iterations, or the loss of desirable conservation properties. As a result, their applicability to high-order

conservative transport simulations remains restricted.

Over the past decade, motivated by the increasing use of high-order DG schemes for transport, the development of positivity-preserving techniques have increasingly emphasized the simultaneous maintenance of high-order accuracy and the suppression of nonphysical oscillations. It has been shown that high-order DG schemes can be rendered positivity-preserving by combining appropriately designed limiters, such as rotational positivity-preserving limiters together with the linear scaling limiter originally introduced for hyperbolic conservation laws [34]. This strategy yields high-order DG formulations applicable to one- and two-dimensional Cartesian meshes and has later been extended to unstructured triangular meshes [32, 33]. While these approaches can ensure non-negativity together with high-order accuracy, the use of rotational limiters may alter cell averages and thereby compromise local conservation. To overcome this difficulty, it was proved in [17] that, for the radiative transfer equation in one spatial dimension, the DG solution preserves non-negative cell averages. This property allows the direct application of linear scaling limiters without modifying the cell average, thus enforcing positivity while maintaining local conservation. Extensions of this idea to higher dimensions, however, generally require the introduction of augmented polynomial spaces. More recently, Xu and Shu revisited the notion of conservation for positivity-preserving limiters and clarified a more appropriate definition of local mass conservation for stationary hyperbolic problems [30]. Based on this revised definition, they constructed genuinely conservative high-order positivity-preserving DG methods and developed limiter strategies that preserve the defined local mass while maintaining high-order accuracy.

In recent years, several studies have explored how iterative acceleration can be combined with positivity-preserving strategies for radiative transfer problems. The S_2SA preconditioning method for the S_N equations with a strictly nonnegative spatial discretization was investigated in [3]. The quadratic programming flux correction method in [31] guarantees non-negative solutions for high-order DG discretizations of the S_N transport equations and is combined with a variable Eddington factor method for acceleration. These studies show

that iterative acceleration and positivity enforcement can coexist in practical computations. However, the associated acceleration strategies differ from the classical DSA method and may involve additional algorithmic complexity or computational cost. Since diffusion synthetic acceleration remains one of the most efficient techniques for scattering-dominated transport problems, designing a DSA framework compatible with conservative positivity-preserving DG schemes while maintaining fast convergence remains an open challenge.

In this work, we develop a high-order discontinuous Galerkin framework for the S_N radiative transfer equation that integrates diffusion synthetic acceleration with a conservative positivity-preserving strategy. The diffusion correction equation is constructed to be consistent with the discrete diffusion limit of the upwind high-order DG transport scheme and is discretized using a continuous finite element method, following the discrete diffusion-limit analysis of DG transport discretizations [8]. To incorporate the diffusion correction into the high-order DG transport solution, we extend the moment-based P_1 update procedure proposed in [25], originally developed for linear DG discretizations, to high-order DG schemes. This approach determines the DG polynomial coefficients of the diffusion correction from its angular moments obtained from the transport error equation, yielding a representation consistent with the high-order DG transport space and enabling effective diffusion acceleration. A central component of the proposed framework is a conservative positivity-preserving strategy for the radiative transfer equation, which employs limiters that preserve appropriately defined locally conservative quantities. This design enforces non-negativity while maintaining the conservation structure and high-order accuracy of the DG discretization within the accelerated iterative framework. Numerical experiments in one and two spatial dimensions demonstrate that the proposed method achieves accurate solutions, robust positivity preservation, and significantly improved convergence in optically thick and strongly scattering regimes.

The remainder of this paper is organized as follows. In Section 2, we introduce the one- and two-dimensional discrete-ordinate radiative transfer equations and present the corre-

sponding discontinuous Galerkin discretizations together with the source iteration framework. Section 3 is devoted to the diffusion synthetic acceleration method for the DG discretization of the S_N transport equations, where the construction of the acceleration operator is presented in detail. In Section 4, we introduce locally conservative quantities tailored to the DG discretization of the radiative transfer equations and develop high-order positivity-preserving limiters based on this definition. Section 5 presents a series of numerical experiments for both steady-state and time-dependent radiative transfer problems to assess the accuracy, efficiency, and robustness of the proposed method. Finally, conclusions are drawn in Section 6.

2 The radiative transfer equation and its high-order S_N–DG discretization

2.1 One-dimensional radiative transfer equation and its high-order S_N–DG discretization

We first consider the steady radiative transfer equation in one-dimensional slab geometry with isotropic scattering,

$$\mu\,\partial_x\psi(x,\mu)+\Sigma_t\psi(x,\mu)=\frac{\Sigma_s}{2}\int_{-1}^{1}\psi(x,\mu')\,d\mu'+q(x,\mu),\qquad x\in[x_l,x_r],\ \mu\in[-1,1],\quad(2.1)$$

where $\psi(x,\mu)$ denotes the angular radiation intensity in the direction μ. Throughout this work, we assume that the total and scattering cross sections Σ_t and Σ_s are positive constants, with $\Sigma_a=\Sigma_t-\Sigma_s\geqslant 0$ denoting the absorption cross section. The source term is given by $q(x,\mu)$. The inflow boundary conditions are prescribed as

$$\psi(x_l,\mu)=\psi^l(\mu),\quad \mu>0,\qquad \psi(x_r,\mu)=\psi^r(\mu),\quad \mu<0.$$

In particular, a vacuum boundary corresponds to $\psi^l(\mu)=0$ (and analogously at $x=x_r$).

The angular variable is discretized using the discrete-ordinate method with a quadrature set $\{(\mu_m,w_m)\}_{m=1}^{M}$, where μ_m denotes the discrete direction cosine with respect to the spatial

coordinate x, and $w_m > 0$ are the associated quadrature weights satisfying $\sum_{m=1}^{M} w_m = 2$. This yields a coupled system of S_N transport equations

$$\mu_m \, \partial_x \psi_m(x) + \Sigma_t \psi_m(x) = \frac{\Sigma_s}{2} \, \phi(x) + q_m(x), \qquad m = 1, \ldots, M, \tag{2.2}$$

where $\psi_m(x) = \psi(x, \mu_m)$ and $q_m(x) = q(x, \mu_m)$. The scalar flux is defined by

$$\phi(x) = \sum_{m=1}^{M} w_m \, \psi_m(x).$$

We discretize the spatial domain $D = [x_l, x_r]$ into N cells $S_j = [x_{j-\frac{1}{2}}, x_{j+\frac{1}{2}}]$ and introduce the finite element space of piecewise polynomials

$$V_h^k = \{v \in L^2(D) : v|_{S_j} \in \mathbb{P}^k(S_j), \ j = 1, \ldots, N\},$$

where $\mathbb{P}^k(S_j)$ denotes the space of polynomials of degree at most k on S_j.

For each discrete direction m, the DG approximation $\psi_{m,h} \in V_h^k$ is defined by the following formulation: find $\psi_{m,h} \in V_h^k$ such that, for any test function $v \in V_h^k$ and each cell S_j,

$$\begin{aligned} &- \mu_m \int_{S_j} \psi_{m,h}(x) v'(x) dx + \Sigma_t \int_{S_j} \psi_{m,h}(x) v(x) dx + \mu_m \widehat{\psi}_{m,j+\frac{1}{2}} v(x^-_{j+\frac{1}{2}}) - \mu_m \widehat{\psi}_{m,j-\frac{1}{2}} v(x^+_{j-\frac{1}{2}}) \\ =&\frac{\Sigma_s}{2} \int_{S_j} \phi_h(x) v(x) dx + \int_{S_j} q_m(x) v(x) dx, \end{aligned} \tag{2.3}$$

where $\phi_h(x) = \sum_{m'=1}^{M} w_{m'} \psi_{m',h}(x)$ and $\widehat{\psi}_{m,j\pm\frac{1}{2}}$ denotes the numerical flux at the cell interfaces. We employ the standard upwind numerical flux,

$$\widehat{\psi}_{m,j\pm\frac{1}{2}} = \begin{cases} \psi_{m,h}(x^-_{j\pm\frac{1}{2}}), & \mu_m > 0, \\ \psi_{m,h}(x^+_{j\pm\frac{1}{2}}), & \mu_m < 0. \end{cases}$$

With the upwind numerical flux, the DG scheme (2.3) is solved by a directional sweep following the sign of each discrete ordinate. For notational simplicity, in the remainder of this paper we omit the subscript h when referring to the DG approximation.

The equations (2.3) for different discrete directions are coupled through the scattering term involving the scalar flux. To decouple the system, we employ the source iteration

(SI) method. Starting from a given iteration $\{\psi_m^{(\ell)}\}_{m=1}^M$, the next iteration $\{\psi_m^{(\ell+1)}\}_{m=1}^M$ is obtained by solving the DG formulation (2.3) for each discrete direction m. Equivalently, as an example we consider the case $\mu_m > 0$. On each cell S_j one solves

$$
\begin{aligned}
&-\mu_m \int_{S_j} \psi_m^{(\ell+1)}\, v'(x)\, dx + \Sigma_t \int_{S_j} \psi_m^{(\ell+1)}\, v\, dx + \mu_m \psi_m^{(\ell+1)}(x_{j+\frac{1}{2}}^-)\, v(x_{j+\frac{1}{2}}^-) - \mu_m \psi_m^{(\ell+1)}(x_{j-\frac{1}{2}}^+)\, v(x_{j-\frac{1}{2}}^+) \\
=&\frac{\Sigma_s}{2} \int_{S_j} \phi^{(*)}(x)\, v(x)\, dx + \int_{S_j} q_m(x)\, v(x)\, dx,
\end{aligned}
$$

where the scattering source is evaluated using the most recently available angular fluxes, following a standard Gauss–Seidel source iteration. For each iteration, the angular equations are solved by a directional sweep through the spatial cells following the upwind order associated with each discrete direction, so that the required upstream interface values are always available from either the boundary conditions or previously updated cells. Further details on efficient grid sweeping strategies can be found in [32].

The iteration is terminated when

$$
\max_{1\leqslant m\leqslant M} \max_{1\leqslant j\leqslant N} \left\| \psi_m^{(\ell+1)} - \psi_m^{(\ell)} \right\|_{L^\infty(S_j)} \leqslant \varepsilon_{\mathrm{SI}}.
$$

where $\varepsilon_{\mathrm{SI}}$ is a prescribed parameter defining the stopping criterion.

We now turn to the unsteady radiative transfer equation,

$$
\frac{1}{c}\frac{\partial \psi(x,\mu,t)}{\partial t} + \mu \frac{\partial \psi(x,\mu,t)}{\partial x} + \Sigma_t \psi(x,\mu,t) = \frac{\Sigma_s}{2} \int_{-1}^{1} \psi(x,\mu',t)\, d\mu' + q(x,\mu,t), \tag{2.4}
$$

where c denotes the speed of light, and the equation is supplemented with the corresponding inflow boundary conditions and an initial condition $\psi(x,\mu,0) = \psi_0(x,\mu)$.

To discretize the temporal variable, a backward Euler time discretization is employed. This implicit treatment avoids the severe stability restriction of explicit time stepping, since the transport problem involves the high speed c, which induces a CFL-type condition $\Delta t = O(1/c)$ and consequently requires prohibitively small time steps. At each time step, the fully discrete system takes the same spatial form as (2.2), with the modified coefficients

$$
\widetilde{\Sigma}_t = \Sigma_t + \frac{1}{c\Delta t}, \qquad \widetilde{q}_m(x) = q_m(x, t_{n+1}) + \frac{1}{c\Delta t}\psi_m(x, t_n).
$$

As a result, the DG discretization and source iteration procedure for the unsteady problem are algebraically identical to those of the steady case. Therefore, in the remainder of this paper we focus on the steady formulation without loss of generality.

2.2 Two-dimensional radiative transfer equation and its high-order S_N–DG discretization

We next consider the radiative transfer equation in two spatial dimensions with isotropic scattering. In steady state, the equation reads

$$\boldsymbol{\Omega} \cdot \nabla_{\boldsymbol{r}} \psi(\boldsymbol{r}, \boldsymbol{\Omega}) + \Sigma_t \psi(\boldsymbol{r}, \boldsymbol{\Omega}) = \frac{\Sigma_s}{4\pi} \int_{\mathbb{S}^2} \psi(\boldsymbol{r}, \boldsymbol{\Omega}')\, d\boldsymbol{\Omega}' + q(\boldsymbol{r}, \boldsymbol{\Omega}), \tag{2.5}$$

where $\boldsymbol{r} = (x, y) \in D \subset \mathbb{R}^2$ denotes the spatial position and $\boldsymbol{\Omega} \in \mathbb{S}^2$ is the angular direction, with $\mathbb{S}^2$ denoting the unit sphere. The function $\psi(\boldsymbol{r}, \boldsymbol{\Omega})$ represents the angular radiation intensity, and $q(\boldsymbol{r}, \boldsymbol{\Omega})$ is a prescribed source term.

For two-dimensional x-y geometry, the angular variable $\boldsymbol{\Omega}$ is commonly parameterized by the polar angle $\varphi \in [0, \pi]$ and the azimuthal angle $\theta \in [0, 2\pi)$. Introducing $\mu = \cos\varphi$, the surface measure on the unit sphere satisfies

$$d\boldsymbol{\Omega} = \sin\varphi \, d\varphi \, d\theta = -\, d\mu \, d\theta.$$

In two spatial dimensions, the S_N discretization is constructed using Chebyshev–Legendre (CL) quadrature rules. Specifically, the angular quadrature is formed as a tensor product of a Chebyshev rule on the unit circle for the azimuthal angle and a Gauss–Legendre rule on $[-1, 1]$ for the polar cosine μ. The quadrature set is denoted by $\{(\boldsymbol{\Omega}_m, w_m)\}_{m=1}^{M}$ with $\sum_{m=1}^{M} w_m = 4\pi$, and we write the corresponding x-y direction cosines as $\boldsymbol{\Omega}_m = (\mu_m, \lambda_m)$. Applying the S_N method to (2.5) yields the following system of transport equations in Cartesian coordinates:

$$\mu_m \, \partial_x \psi_m(x, y) + \lambda_m \, \partial_y \psi_m(x, y) + \Sigma_t \psi_m(x, y) = \frac{\Sigma_s}{4\pi} \, \phi(x, y) + q_m(x, y), \quad m = 1, \ldots, M, \tag{2.6}$$

where $\psi_m(x,y) = \psi(\boldsymbol{r}, \boldsymbol{\Omega}_m)$, $q_m(x,y) = q(\boldsymbol{r}, \boldsymbol{\Omega}_m)$, and the scalar flux is defined by $\phi(x,y) = \sum_{m=1}^{M} w_m \, \psi_m(x,y)$.

We discretize the computational domain $D = [a,b] \times [c,d]$ using a Cartesian mesh of rectangular cells $S_{i,j} = [x_{i-\frac{1}{2}}, x_{i+\frac{1}{2}}] \times [y_{j-\frac{1}{2}}, y_{j+\frac{1}{2}}]$, $i = 1, \ldots, N_x$, $j = 1, \ldots, N_y$, and introduce the discontinuous finite element space $V_h^k = \{ v \in L^2(D) : v|_{S_{i,j}} \in \mathbb{P}^k(S_{i,j}), \ \forall \, i,j \}$. For a given discrete direction (μ_m, λ_m), the DG approximation $\psi_m \in V_h^k$ is defined by a local weak formulation on each cell, with upwind numerical fluxes at cell interfaces. As an example, we present the case $\mu_m > 0$ and $\lambda_m > 0$. Find $\psi_m \in V_h^k$ such that for any test function $v \in V_h^k$ and each cell $S_{i,j}$,

$$
\begin{aligned}
&- \int_{S_{i,j}} \psi_m (\mu_m \, \partial_x v + \lambda_m \, \partial_y v) \, dx \, dy + \Sigma_t \int_{S_{i,j}} \psi_m \, v \, dx \, dy \\
&+ \mu_m \int_{y_{j-\frac{1}{2}}}^{y_{j+\frac{1}{2}}} \psi_m(x^-_{i+\frac{1}{2}}, y) \, v(x^-_{i+\frac{1}{2}}, y) \, dy + \lambda_m \int_{x_{i-\frac{1}{2}}}^{x_{i+\frac{1}{2}}} \psi_m(x, y^-_{j+\frac{1}{2}}) \, v(x, y^-_{j+\frac{1}{2}}) \, dx \\
&\qquad = \frac{\Sigma_s}{4\pi} \int_{S_{i,j}} \phi \, v \, dx \, dy + \int_{S_{i,j}} q_m \, v \, dx \, dy \\
&+ \mu_m \int_{y_{j-\frac{1}{2}}}^{y_{j+\frac{1}{2}}} \psi_m(x^-_{i-\frac{1}{2}}, y) \, v(x^+_{i-\frac{1}{2}}, y) \, dy + \lambda_m \int_{x_{i-\frac{1}{2}}}^{x_{i+\frac{1}{2}}} \psi_m(x, y^-_{j-\frac{1}{2}}) \, v(x, y^+_{j-\frac{1}{2}}) \, dx.
\end{aligned}
$$

The formulations for the other combinations of (μ_m, λ_m) are obtained in a completely analogous manner. For each discrete direction, the angular equation is solved by a directional sweep starting from the inflow boundary corner determined by the sign of (μ_m, λ_m).

Similarly to the one-dimensional case, the angular equations are solved by source iteration, where the scattering source is evaluated using the most recently available angular fluxes following a Gauss–Seidel strategy.

For the time-dependent problem, the unsteady radiative transfer equation in two spatial dimensions is given by

$$
\frac{1}{c} \, \partial_t \psi(\boldsymbol{r}, \boldsymbol{\Omega}, t) + \boldsymbol{\Omega} \cdot \nabla_{\boldsymbol{r}} \psi(\boldsymbol{r}, \boldsymbol{\Omega}, t) + \Sigma_t \psi(\boldsymbol{r}, \boldsymbol{\Omega}, t) = \frac{\Sigma_s}{4\pi} \int_{\mathbb{S}^2} \psi(\boldsymbol{r}, \boldsymbol{\Omega}', t) \, d\boldsymbol{\Omega}' + q(\boldsymbol{r}, \boldsymbol{\Omega}, t), \quad (2.7)
$$

supplemented with appropriate inflow boundary conditions and an initial condition. A backward Euler discretization in time leads to a fully discrete system that has the same spatial

structure as the steady formulation (2.6). At each time step, the fully discrete system takes the same spatial form as the steady problem (2.6), with modified coefficients

$$\widetilde{\Sigma}_t = \Sigma_t + \frac{1}{c\Delta t}, \qquad \widetilde{q}_m(x,y) = q_m(x,y,t_{n+1}) + \frac{1}{c\Delta t}\psi_m(x,y,t_n).$$

Consequently, the DG discretization and source iteration procedure for the unsteady problem are algebraically identical to those of the steady case, and we focus on the steady formulation in the subsequent analysis.

3 Accelerated iterative methods for the S_N radiative transfer equations

In optically thick and strongly scattering regimes, the conventional SI for the S_N discretization of the radiative transfer equation may converge extremely slowly. Diffusion synthetic acceleration addresses this difficulty by approximating the slowly decaying error modes of SI with a diffusion equation and using the resulting correction to accelerate the outer iteration. In this section, we follow the DSA framework originally proposed by Wareing [25] for linear discontinuous Galerkin discretizations, and extend it to the high-order DG setting considered in this work. The resulting acceleration strategy is guided by the asymptotic diffusive-limit analysis of upwind high-order DG transport schemes and provides the acceleration foundation for the positivity-preserving framework developed in the next section.

3.1 A four-step DSA procedure at the continuous level

We briefly recall the standard DSA procedure for the steady S_N transport problem at the continuous level, which applies to both one-dimensional slab geometry and two-dimensional Cartesian domains.

Let $\{\mathbf{\Omega}_m, w_m\}_{m=1}^M$ denote a discrete ordinate quadrature set, and let $\psi_m(\mathbf{x})$ and $\phi(\mathbf{x})$ denote the angular and scalar fluxes, respectively. A single iteration from level ℓ to $\ell+1$ consists of the following four steps.

Step 1 (transport sweep). Given $\phi^{(\ell)}$, compute the intermediate angular flux $\psi_m^{(\ell+1/2)}$ by solving

$$\mathbf{\Omega}_m \cdot \nabla \psi_m^{(\ell+1/2)}(\mathbf{x}) + \Sigma_t \, \psi_m^{(\ell+1/2)}(\mathbf{x}) = \frac{\Sigma_s}{C} \, \phi^{(\ell)}(\mathbf{x}) + q_m(\mathbf{x}),$$

for $m = 1, \ldots, M$, subject to vacuum inflow boundary conditions. Here, C denotes the normalization constant associated with the isotropic scattering operator.

Step 2 (scalar flux update). Update the intermediate scalar flux by angular quadrature,

$$\phi^{(\ell+1/2)}(\mathbf{x}) = \sum_{m=1}^{M} w_m \, \psi_m^{(\ell+1/2)}(\mathbf{x}).$$

Step 3 (diffusion correction). Compute the scalar flux correction $f^{(\ell+1)}$ by solving the diffusion equation

$$-\nabla \cdot \big(\tfrac{1}{3\Sigma_t} \nabla f^{(\ell+1)}\big) + \Sigma_a \, f^{(\ell+1)} = \Sigma_s \big(\phi^{(\ell+1/2)} - \phi^{(\ell)}\big), \qquad \mathbf{x} \in D, \tag{3.1}$$

supplemented with appropriate boundary conditions.

Step 4 (DSA update). Update the scalar flux according to

$$\phi^{(\ell+1)} = \phi^{(\ell+1/2)} + f^{(\ell+1)}. \tag{3.2}$$

At the continuous level, the DSA correction consists of adding the diffusion-based error estimate to the intermediate scalar flux. The consistent incorporation of this correction into high-order DG discretizations is addressed in subsequent subsections.

3.2 Diffusive limit analysis for upwind high-order DG transport and the resulting diffusion discretization

In optically thick scattering regimes, a standard diffusive scaling introduces a small parameter $\varepsilon \ll 1$ such that

$$\Sigma_t \mapsto \frac{\Sigma_t}{\varepsilon}, \qquad \Sigma_s \mapsto \frac{\Sigma_t}{\varepsilon} - \varepsilon \, \Sigma_a, \qquad q \mapsto \varepsilon \, q, \tag{3.3}$$

so that the mean free path is $\mathcal{O}(\varepsilon)$ and scattering dominates as $\varepsilon \to 0$. At the continuous level, this scaling leads to the classical diffusion limit, in which the leading-order angular dependence is isotropic and the scalar flux satisfies the diffusion equation.

For DSA, however, the diffusion limit must be examined at the discrete level of the transport discretization. It has long been recognized that the effectiveness and robustness of DSA depend on the consistency between the discretization of the diffusion correction equation and the discretization of the S_N transport problem [11]. In particular, the diffusion equation employed in the acceleration procedure should reflect the asymptotic diffusion behavior of the discretized transport formulation. When this consistency is violated, the diffusion correction may fail to capture the slowly converging components of the source iteration error, leading to degraded acceleration or loss of stability.

A rigorous analysis of the discrete diffusion limit for upwind DG transport discretizations was established in [8]. Under the diffusive scaling (3.3), the discrete angular flux admits the formal expansion

$$\psi = \psi^{(0)} + \varepsilon\, \psi^{(1)} + \mathcal{O}(\varepsilon^2),$$

where the leading-order term $\psi^{(0)}$ is isotropic and determined by the corresponding discrete scalar flux. A key structural result in [8] is that the upwind DG discretization yields the correct discrete diffusion limit if and only if its approximation space contains a subspace of functions that are continuous across element interfaces and include at least piecewise linear polynomials on each cell.

This observation provides the basis for the construction of the diffusion operator used in the DSA procedure. In particular, the asymptotic analysis in [8] implies that, on both one-dimensional meshes and two-dimensional rectangular meshes, the discrete diffusion limit of the upwind DG transport operator corresponds to a continuous finite element discretization of the diffusion equation. Notably, this diffusion discretization coincides with the form of the correction equation employed in the DSA framework proposed by Wareing [25] for linear DG transport schemes.

Motivated by this correspondence, the diffusion correction equation (3.1) is discretized using a continuous finite element space V_h^c defined on a mesh $\mathcal{T}_h$ consisting of intervals in one dimension or rectangles in two dimensions. Specifically, the diffusion correction $f^{(\ell+1)}$ is approximated in V_h^c by the standard weak formulation: find $f^{(\ell+1)} \in V_h^c$ such that, for all $v \in V_h^c$,

$$\int_D \frac{1}{3\Sigma_t} \nabla f^{(\ell+1)} \cdot \nabla v \, \mathrm{d}\mathbf{x} + \int_D \Sigma_a f^{(\ell+1)} v \, \mathrm{d}\mathbf{x} + \int_{\partial D} \alpha f^{(\ell+1)} v \, \mathrm{d}s = \int_D \Sigma_s \left(\phi^{(\ell+1/2)} - \phi^{(\ell)}\right) v \, \mathrm{d}\mathbf{x} + \int_{\partial D} g v \, \mathrm{d}s.$$

The boundary terms (α, g) arise from the weak imposition of the Robin-type boundary conditions and will be specified in the latter for the vacuum boundaries considered in this work.

In the numerical implementation, the diffusion correction is discretized in a continuous finite element space and coupled with upwind high-order DG discretizations of the S_N transport equations. In one spatial dimension, the transport sweep and diffusion correction naturally employ the same polynomial degree, namely P^1 and P^2 in the second- and third-order cases. In two spatial dimensions, to satisfy the continuity requirement underlying the discrete diffusion-limit analysis of upwind DG schemes [8], the diffusion correction equation is discretized using a continuous Q^1 finite element space, while the transport equations are approximated by Q^1 and P^2 upwind DG discretizations. This choice is compatible with the discrete diffusion-limit structure associated with upwind DG transport discretizations and allows the DSA framework of [25], originally developed for linear DG schemes, to be applied in the high-order DG setting considered here.

The diffusion equation employed in the DSA procedure must be supplied with boundary conditions obtained from the diffusion-limit analysis of the transport equation. For vacuum inflow conditions, classical asymptotic theory shows that the appropriate boundary condition is derived by performing a boundary-layer analysis near the domain boundary and matching the interior diffusion solution with boundary-layer solutions [12]. This procedure results in a Robin-type boundary condition for the scalar flux. In the present work, the diffusion

correction $f^{(\ell+1)}$ satisfies the following boundary condition on ∂D:

$$f^{(\ell+1)} + \frac{2}{3\Sigma_t}\,\mathbf{n}\cdot\nabla f^{(\ell+1)} = 0,$$

where $\mathbf{n}$ denotes the outward unit normal vector on ∂D. Within the weak formulation given above, this boundary condition corresponds to the choice $\alpha = \frac{1}{2}$ and $g = 0$.

3.3 P_1-based update of diffusion corrections for DG discretization of the S_N transport equations

After solving the diffusion correction equation, the resulting scalar correction must be incorporated into the upwind DG transport solver through the scalar update (3.2). For DG transport discretizations, the effectiveness of DSA depends on how the correction is represented in the DG polynomial space. In particular, directly using the polynomial obtained from the diffusion solve does not in general provide an effective acceleration, because this correction does not account for the discrete structure of the transport error equation corresponding to the DG discretization. It was shown in [25] that for linear DG schemes such a direct treatment may fail to reduce the spectral radius of the source iteration and can even lead to values close to unity, resulting in little or no acceleration. To address this issue, a moment-based P_1 update procedure was introduced to determine the DG coefficients of the correction using angular moment information derived from the transport error equation, thereby recovering an effective acceleration mechanism.

Following this approach, we adopt the moment-based P_1 update strategy originally proposed for linear DG transport discretizations and extend it to the high-order DG schemes considered here. The objective of this subsection is to derive algebraic relations that determine the DG coefficients of the diffusion correction from the scalar diffusion solution. Here P_1 refers to the first-order spherical harmonics (P_N) truncation of the angular dependence and should be distinguished from the spatial polynomial space P^k used in the DG discretization. To determine the DG representation of the correction, we make use of the transport error

equation satisfied by the correction under the DG discretization. Taking the discrete zeroth and first angular moments of this DG formulation yields relations for the scalar correction and the corresponding first angular moment of the angular correction. The angular correction is then approximated using a truncated P_1 expansion, which allows the DG coefficients of the correction to be expressed in terms of these moment variables and the corresponding interface values. The resulting update procedure constitutes the key acceleration component of the present method.

We introduce the angular correction increment

$$F_m^{(\ell+1)}(x) := \psi_m^{(\ell+1)}(x) - \psi_m^{(\ell+\frac{1}{2})}(x),$$

which represents the change between the intermediate transport solution and the DSA-updated angular flux in direction μ_m. The corresponding scalar correction $f^{(\ell+1)}(x)$ and first angular moment correction $J^{(\ell+1)}(x)$ are defined as

$$f^{(\ell+1)}(x) = \sum_{m=1}^{M} w_m F_m^{(\ell+1)}(x), \qquad J^{(\ell+1)}(x) = \sum_{m=1}^{M} \mu_m w_m F_m^{(\ell+1)}(x).$$

Here $f^{(\ell+1)}(x)$ is the discrete zeroth angular moment of the correction, and $J^{(\ell+1)}(x)$ denotes the corresponding first angular moment.

For definiteness, we consider the one-dimensional steady S_N transport equation discretized by a P^2-DG method. On each cell $S_j = [x_{j-\frac{1}{2}}, x_{j+\frac{1}{2}}]$, the angular correction is approximated by

$$F_m^{(\ell+1)}(x)\big|_{S_j} = F_{m,j}^{(\ell+1)} + \frac{2}{\triangle x}(x - x_j)\hat{F}_{m,j}^{(\ell+1)} + \frac{4}{\triangle x^2}(x - x_j)^2 \hat{\hat{F}}_{m,j}^{(\ell+1)},$$

where $F_{m,j}^{(\ell+1)}$, $\hat{F}_{m,j}^{(\ell+1)}$, and $\hat{\hat{F}}_{m,j}^{(\ell+1)}$ are the coefficients associated with the local P^2 DG basis functions $\{1, \frac{2(x-x_j)}{\triangle x}, \frac{4(x-x_j)^2}{\triangle x^2}\}$. Analogous polynomial expansions are used for the scalar correction $f^{(\ell+1)}(x)$ and the first angular moment $J^{(\ell+1)}(x)$, with corresponding coefficients $f_j^{(\ell+1)}$, $\hat{f}_j^{(\ell+1)}$, $\hat{\hat{f}}_j^{(\ell+1)}$ and $J_j^{(\ell+1)}$, $\hat{J}_j^{(\ell+1)}$, $\hat{\hat{J}}_j^{(\ell+1)}$.

Next, we substitute the above expansions into the DG formulation of the transport error equation. By choosing the same local basis functions for the test functions as used for the

unknowns, we obtain three equations on each cell S_j corresponding to these basis functions. Written in terms of the DG coefficients, the resulting relations take the form

$$\begin{aligned}
&\frac{\mu_m}{\triangle x}\left(F^{(\ell+1)}_{m,j+\frac{1}{2}} - F^{(\ell+1)}_{m,j-\frac{1}{2}}\right) + \Sigma_t\left(F^{(\ell+1)}_{m,j} + \frac{1}{3}\hat{\hat{F}}^{(\ell+1)}_{m,j}\right) = \frac{\Sigma_s}{2}\left(f_j^{(\ell+1)} + f_j^{(\ell+\frac{1}{2})} + \frac{1}{3}\hat{\hat{f}}_j^{(\ell+1)} + \frac{1}{3}\hat{\hat{f}}_j^{(\ell+\frac{1}{2})}\right),\\
&\frac{3\mu_m}{\triangle x}\left(F^{(\ell+1)}_{m,j+\frac{1}{2}} + F^{(\ell+1)}_{m,j-\frac{1}{2}} - 2F^{(\ell+1)}_{m,j} - \frac{2}{3}\hat{\hat{F}}^{(\ell+1)}_{m,j}\right) + \Sigma_t\hat{F}^{(\ell+1)}_{m,j} = \frac{\Sigma_s}{2}\left(\hat{f}_j^{(\ell+1)} + \hat{f}_j^{(\ell+\frac{1}{2})}\right),\\
&\frac{\mu_m}{\triangle x}\left(F^{(\ell+1)}_{m,j+\frac{1}{2}} - F^{(\ell+1)}_{m,j-\frac{1}{2}} - \frac{4}{3}\hat{F}^{(\ell+1)}_{m,j}\right) + \Sigma_t\left(\frac{1}{3}F^{(\ell+1)}_{m,j} + \frac{1}{5}\hat{\hat{F}}^{(\ell+1)}_{m,j}\right)\\
=&\frac{\Sigma_s}{2}\left(\frac{1}{3}f_j^{(\ell+1)} + \frac{1}{3}f_j^{(\ell+\frac{1}{2})} + \frac{1}{5}\hat{\hat{f}}_j^{(\ell+1)} + \frac{1}{5}\hat{\hat{f}}_j^{(\ell+\frac{1}{2})}\right),
\end{aligned} \tag{3.4}$$

where $F^{(\ell+1)}_{m,j\pm\frac{1}{2}}$ denote the corresponding interface values of the DG approximation at $x_{j\pm\frac{1}{2}}$. The quantities with superscript $(\ell+\frac{1}{2})$ denote the DG coefficients of the scalar flux difference at the intermediate transport level, i.e., those associated with the difference $\phi^{(\ell+\frac{1}{2})}(x) - \phi^{(\ell)}(x)$. The interface values are determined using the standard upwind rule:

$$\mu_m > 0:\ F^{(\ell+1)}_{m,j+\frac{1}{2}} = F^{(\ell+1)}_{m,j} + \hat{F}^{(\ell+1)}_{m,j} + \hat{\hat{F}}^{(\ell+1)}_{m,j}, \quad \mu_m < 0:\ F^{(\ell+1)}_{m,j-\frac{1}{2}} = F^{(\ell+1)}_{m,j} - \hat{F}^{(\ell+1)}_{m,j} + \hat{\hat{F}}^{(\ell+1)}_{m,j}. \tag{3.5}$$

Then we take the discrete zeroth angular moment of (3.4), defined by $\sum_{m=1}^{M} w_m(\cdot)$, yielding the following relations for the scalar correction f and the first angular moment J:

$$\begin{aligned}
&\frac{1}{\triangle x}\left(J^{(\ell+1)}_{j+\frac{1}{2}} - J^{(\ell+1)}_{j-\frac{1}{2}}\right) + \Sigma_a\left(f_j^{(\ell+1)} + \frac{1}{3}\hat{\hat{f}}_j^{(\ell+1)}\right) = \Sigma_s\left(f_j^{(\ell+\frac{1}{2})} + \frac{1}{3}\hat{\hat{f}}_j^{(\ell+\frac{1}{2})}\right),\\
&\frac{3}{\triangle x}\left(J^{(\ell+1)}_{j+\frac{1}{2}} + J^{(\ell+1)}_{j-\frac{1}{2}} - 2J_j^{(\ell+1)} - \frac{2}{3}\hat{\hat{J}}_j^{(\ell+1)}\right) + \Sigma_a\hat{f}_j^{(\ell+1)} = \Sigma_s\hat{f}_j^{(\ell+\frac{1}{2})},\\
&\frac{1}{\triangle x}\left(J^{(\ell+1)}_{j+\frac{1}{2}} - J^{(\ell+1)}_{j-\frac{1}{2}} - \frac{4}{3}\hat{J}_j^{(\ell+1)}\right) + \Sigma_a\left(\frac{1}{3}f_j^{(\ell+1)} + \frac{1}{5}\hat{\hat{f}}_j^{(\ell+1)}\right) = \Sigma_s\left(\frac{1}{3}f_j^{(\ell+\frac{1}{2})} + \frac{1}{5}\hat{\hat{f}}_j^{(\ell+\frac{1}{2})}\right).
\end{aligned} \tag{3.6}$$

Taking the discrete first angular moment of (3.4), defined by $\sum_{m=1}^{M} \mu_m w_m(\cdot)$, introduces the second angular moment of the angular correction through terms of the form $\sum_m \mu_m^2 w_m F_m$. Consequently, the resulting relations involve higher-order angular moments and therefore cannot be written solely in terms of the scalar correction f and the first angular moment J.

To express the relations solely in terms of the zeroth and first angular moments f and J, we approximate the angular dependence of the correction using the truncated P_1 representation

$$F_m(x) \approx \frac{1}{2}f(x) + \frac{3}{2}\mu_m J(x), \tag{3.7}$$

which represents the angular correction in terms of its zeroth and first angular moments.

Substituting the approximation (3.7) into the first angular moment relations and using the symmetry properties of the quadrature set, the resulting equations reduce to

$$\begin{aligned}
&\frac{1}{3\triangle x}\left(f_{j+\frac{1}{2}}^{(\ell+1)}-f_{j-\frac{1}{2}}^{(\ell+1)}\right)+\Sigma_t\left(J_j^{(\ell+1)}+\frac{1}{3}\hat{\hat{f}}_j^{(\ell+1)}\right)=0,\\
&\frac{1}{\triangle x}\left(f_{j+\frac{1}{2}}^{(\ell+1)}+f_{j-\frac{1}{2}}^{(\ell+1)}-2f_j^{(\ell+1)}-\frac{2}{3}\hat{\hat{f}}_j^{(\ell+1)}\right)+\Sigma_t\hat{J}_j^{(\ell+1)}=0,\\
&\frac{1}{3\triangle x}\left(f_{j+\frac{1}{2}}^{(\ell+1)}-f_{j-\frac{1}{2}}^{(\ell+1)}-\frac{4}{3}\hat{f}_j^{(\ell+1)}\right)+\Sigma_t\left(\frac{1}{3}J_j^{(\ell+1)}+\frac{1}{5}\hat{\hat{J}}_j^{(\ell+1)}\right)=0.
\end{aligned}\tag{3.8}$$

We similarly take the discrete zeroth and first angular moments of the interface relations (3.5). Applying the truncated P_1 approximation (3.7) and using the symmetry of the angular quadrature, we obtain the following identities relating the interface values and the DG coefficients:

$$\begin{aligned}
&\frac{1}{2}\left(f_{j+\frac{1}{2}}^{(\ell+1)}+f_{j-\frac{1}{2}}^{(\ell+1)}\right)+\frac{3\delta}{4}\left(J_{j+\frac{1}{2}}^{(\ell+1)}-J_{j-\frac{1}{2}}^{(\ell+1)}\right)=f_j^{(\ell+1)}+\hat{\hat{f}}_j^{(\ell+1)}+\frac{3\delta}{2}\hat{J}_j^{(\ell+1)},\\
&\frac{1}{2}\left(J_{j+\frac{1}{2}}^{(\ell+1)}+J_{j-\frac{1}{2}}^{(\ell+1)}\right)+\frac{\delta}{4}\left(f_{j+\frac{1}{2}}^{(\ell+1)}-f_{j-\frac{1}{2}}^{(\ell+1)}\right)=J_j^{(\ell+1)}+\hat{\hat{J}}_j^{(\ell+1)}+\frac{\delta}{2}\hat{f}_j^{(\ell+1)}.
\end{aligned}\tag{3.9}$$

where $\delta=2\sum\limits_{\mu_m>0}\mu_m w_m$.

Together with the moment relations (3.6)–(3.8), the identities (3.9) form a local algebraic system on each cell S_j for the DG coefficients of the scalar correction $f^{(\ell+1)}$. This system determines the coefficients $\left(f_j^{(\ell+1)},\hat{f}_j^{(\ell+1)},\hat{\hat{f}}_j^{(\ell+1)}\right)$ from the interface values $f_{j\pm\frac{1}{2}}^{(\ell+1)}$ together with the known coefficients of the intermediate correction $f^{(\ell+\frac{1}{2})}$. At this stage, the interface values $f_{j\pm\frac{1}{2}}^{(\ell+1)}$ are already available from the continuous finite element approximation of the diffusion correction equation, and the coefficients of the intermediate correction $f^{(\ell+\frac{1}{2})}$ are known from the transport half step. The remaining task is therefore to determine the DG coefficients $f_j^{(\ell+1)},\hat{f}_j^{(\ell+1)},\hat{\hat{f}}_j^{(\ell+1)}$ of the scalar correction on each cell S_j.

Using the above relations, the first angular moment coefficients can first be eliminated to obtain a scalar equation for $\hat{f}_j^{(\ell+1)}$:

$$\left(1+\frac{20}{3\delta\Sigma_t\triangle x}+\frac{\Sigma_a\triangle x}{3\delta}\right)\hat{f}_j^{(\ell+1)}=\left(\frac{1}{2}+\frac{10}{3\delta\Sigma_t\triangle x}\right)\left(f_{j+\frac{1}{2}}^{(\ell+1)}-f_{j-\frac{1}{2}}^{(\ell+1)}\right)+\frac{\Sigma_s\triangle x}{3\delta}\hat{f}_j^{(\ell+\frac{1}{2})}.$$

The same elimination procedure yields a coupled 2×2 linear system for the remaining

two coefficients $f_j^{(\ell+1)}$ and $\hat{\hat{f}}_j^{(\ell+1)}$:

$$a_1 f_j^{(\ell+1)} + a_2 \hat{\hat{f}}_j^{(\ell+1)} = a_3 \left(f_{j+\frac{1}{2}}^{(\ell+1)} + f_{j-\frac{1}{2}}^{(\ell+1)} \right) + \Sigma_s \left(f_j^{(\ell+\frac{1}{2})} + \frac{1}{3} \hat{\hat{f}}_j^{(\ell+\frac{1}{2})} \right),$$
$$b_1 f_j^{(\ell+1)} + b_2 \hat{\hat{f}}_j^{(\ell+1)} = b_3 \left(f_{j+\frac{1}{2}}^{(\ell+1)} + f_{j-\frac{1}{2}}^{(\ell+1)} \right) + \Sigma_s \left(\frac{1}{3} f_j^{(\ell+\frac{1}{2})} + \frac{1}{5} \hat{\hat{f}}_j^{(\ell+\frac{1}{2})} \right),$$

where

$$a_1 = \frac{4}{3\delta\triangle x} + \frac{4}{\Sigma_t(\triangle x)^2} + \Sigma_a,\ a_2 = \frac{4}{3\delta\triangle x} + \frac{4}{3\Sigma_t(\triangle x)^2} + \frac{\Sigma_a}{3},\ a_3 = \frac{2}{3\delta\triangle x} + \frac{2}{\Sigma_t(\triangle x)^2},$$
$$b_1 = \frac{4}{3\delta\triangle x} + \frac{4}{3\Sigma_t(\triangle x)^2} + \frac{\Sigma_a}{3},\ b_2 = \frac{4}{3\delta\triangle x} + \frac{4}{9\Sigma_t(\triangle x)^2} + \frac{\Sigma_a}{5},\ b_3 = \frac{2}{3\delta\triangle x} + \frac{2}{3\Sigma_t(\triangle x)^2}.$$

Solving this 2×2 system and combining the result with the expression for $\hat{f}_j^{(\ell+1)}$ gives the DG coefficients of the scalar correction in explicit form:

$$f_j^{(\ell+1)} = \left[\beta_{1,1} f_j^{(\ell+\frac{1}{2})} + \beta_{1,3} \hat{\hat{f}}_j^{(\ell+\frac{1}{2})} + \gamma_1 \left(f_{j+\frac{1}{2}}^{(\ell+1)} + f_{j-\frac{1}{2}}^{(\ell+1)} \right) \right] / \alpha_1,$$
$$\hat{f}_j^{(\ell+1)} = \left[\Sigma_s \hat{f}_j^{(\ell+\frac{1}{2})} + \gamma_2 \left(f_{j+\frac{1}{2}}^{(\ell+1)} - f_{j-\frac{1}{2}}^{(\ell+1)} \right) \right] / \alpha_2,$$
$$\hat{\hat{f}}_j^{(\ell+1)} = \left[\beta_{3,1} f_j^{(\ell+\frac{1}{2})} + \beta_{3,3} \hat{\hat{f}}_j^{(\ell+\frac{1}{2})} + \gamma_3 \left(f_{j+\frac{1}{2}}^{(\ell+1)} + f_{j-\frac{1}{2}}^{(\ell+1)} \right) \right] / \alpha_1,$$

with

$$\alpha_1 = (a_1 b_2 - a_2 b_1),\ \alpha_2 = \frac{3\delta}{\triangle x} + \frac{20}{\Sigma_t(\triangle x)^2} + \Sigma_a,\ \gamma_1 = (b_2 a_3 - a_2 b_3),\ \gamma_2 = \alpha_2 - \Sigma_a,\ \gamma_3 = (a_1 b_3 - b_1 a_3),$$
$$\beta_{1,1} = \Sigma_s \left(b_2 - \frac{1}{3} a_2 \right),\ \beta_{1,3} = \Sigma_s \left(\frac{1}{3} b_2 - \frac{1}{5} a_2 \right),\ \beta_{3,1} = \Sigma_s \left(-b_1 + \frac{1}{3} a_1 \right),\ \beta_{3,3} = \Sigma_s \left(-\frac{1}{3} b_1 + \frac{1}{5} a_1 \right).$$

These formulas provide a local update of the DG coefficients of the scalar correction from the interface values supplied by the continuous diffusion solve and the known intermediate coefficients. The scalar flux is then updated by $\phi^{(\ell+1)} = \phi^{(\ell+\frac{1}{2})} + f^{(\ell+1)}$.

The extension to two spatial dimensions follows the same moment-based construction and leads to an analogous local algebraic system for the coefficients of the high-order DG approximation.

4 High-order positivity-preserving and conservative method for accelerated radiative transfer solutions

For radiative transfer equations with non-negative source terms and inflow boundary conditions, the radiation intensity is required to remain non-negative to ensure physical admissibility and numerical stability. However, high-order discretizations are prone to producing spurious negative values, especially in the presence of strong gradients or highly scattering regimes.

A systematic framework for constructing positivity-preserving and conservative numerical methods for stationary hyperbolic equations has recently been developed by Xu and Shu [30]. When the S_N transport equations are solved by standard source iteration, their algebraic structure closely resembles that of stationary hyperbolic systems, which allows the Xu-Shu positivity-preserving strategy to be applied directly at each iteration step. In the presence of diffusion synthetic acceleration, however, the situation is fundamentally different: enforcing positivity during the accelerated iterations introduces nonlinear modifications that alter the effective iteration operator and may significantly deteriorate the performance of the acceleration. In particular, the framework of [30] is designed for problems with a fixed iteration operator and does not directly extend to accelerated iterations in which diffusion-based corrections are involved.

To overcome this difficulty, we develop a new conservative positivity-preserving strategy specifically tailored to accelerated iterations of the radiative transfer equation. The central idea is to decouple positivity enforcement from the accelerated iteration process itself. The diffusion-accelerated scheme is first iterated to convergence without limiting, after which a positivity-preserving correction is applied as a postprocessing step. The proposed construction consists of two key components: a locally conservative quantity adapted to the accelerated formulation, whose preservation does not affect convergence to the correct weak solution, and a positivity-preserving limiter that enforces non-negativity while maintaining

conservation and the high-order accuracy of the underlying DG discretization.

4.1 Local conservation quantity

We consider the one-dimensional slab geometry and introduce a local conservation quantity for the DG discretization of the steady-state S_N transport equation. The discussion focuses on the case of a given discrete direction with $\mu_m > 0$; the case of $\mu_m < 0$ follows by symmetry. Let $\psi_m(x)|_{S_j}$ denote the converged DG solution on the cell S_j. Then $\psi_m(x)|_{S_j}$ satisfies the following local weak formulation:

$$
\begin{aligned}
&-\mu_m \int_{S_j} \psi_m(x) v'(x)\,dx + \Sigma_t \int_{S_j} \psi_m(x) v(x)\,dx + \mu_m \psi_m(x^-_{j+\frac{1}{2}}) v(x^-_{j+\frac{1}{2}}) \\
&-\frac{\Sigma_s}{2} \int_{S_j} \Big(\sum_{n=1}^{M} w_n \psi_n(x)\Big) v(x)\,dx = \mu_m \psi_m(x^-_{j-\frac{1}{2}})\, v(x^+_{j-\frac{1}{2}}) + \int_{S_j} q_m(x) v(x)\,dx, \qquad \forall v \in V_h^k.
\end{aligned}
$$

Motivated by this formulation, we consider the DG discretization employed in the positivity-preserving procedure. Specifically, after computing the DG solution on each cell, we denote by $\widetilde{\psi}_{m,j}(x)$ the modified solution obtained after applying a positivity-preserving limiter. This modified solution provides the upstream information needed for the subsequent cell update.

Given the modified solution in the upstream cell, we seek $\psi_m(x) \in V_h^k$ on S_j such that

$$
\begin{aligned}
&-\mu_m \int_{S_j} \psi_m(x) v'(x)\,dx + \Sigma_t \int_{S_j} \psi_m(x) v(x)\,dx + \mu_m \psi_m(x^-_{j+\frac{1}{2}}) v(x^-_{j+\frac{1}{2}}) \\
&-\frac{\Sigma_s}{2} \int_{S_j} \Big(\sum_{n=1}^{m-1} w_n \widetilde{\psi}_n(x) + \sum_{n=m}^{M} w_n \psi_n(x)\Big) v(x)\,dx \qquad (4.1) \\
=&\mu_m \widetilde{\psi}_m(x^-_{j-\frac{1}{2}}) v(x^+_{j-\frac{1}{2}}) + \int_{S_j} q_m(x) v(x)\,dx, \qquad \forall v \in V_h^k.
\end{aligned}
$$

For $\mu_m > 0$, the computation of the solution $\psi_{m,j}(x)$ on the cell S_j requires the modified solution from the neighboring upstream cell. In particular, the modified value $\widetilde{\psi}_m(x^-_{j-\frac{1}{2}})$ obtained after positivity correction is used on the right-hand side of (4.1). Once $\psi_{m,j}(x)$ is obtained, a positivity-preserving limiter is applied to construct the modified solution $\widetilde{\psi}_{m,j}(x)$. The resulting modified solution is then used in the computation on the next cell S_{j+1}, and the procedure continues sequentially across the mesh.

Assume that the numerical quadrature used in (4.1) is exact for polynomials of degree k. Taking the test function $v = 1$ on the cell S_j, we obtain the following equation satisfied by the local conservation quantity:

$$\Sigma_t \triangle x\, \overline{\psi}_{m,j} + \mu_m \psi_m(x^-_{j+\frac{1}{2}}) - \frac{\Sigma_s}{2}\triangle x\Big(\sum_{n=1}^{m-1} w_n \overline{\widetilde{\psi}}_{n,j} + \sum_{n=m}^{M} w_n \overline{\psi}_{n,j}\Big) = \mu_m \widetilde{\psi}_m(x^-_{j-\frac{1}{2}}) + \triangle x\, \overline{q}_{m,j}, \quad (4.2)$$

where $\overline{\psi}_{m,j}$, $\overline{\widetilde{\psi}}_{n,j}$, and $\overline{q}_{m,j}$ denote the cell averages of ψ_m, $\widetilde{\psi}_n$, and q_m over S_j, respectively.

Motivated by (4.2), we define the local conservation quantity associated with $\psi_{m,j}$ by

$$LHS(\psi_{m,j}) := \Sigma_t \triangle x\, \overline{\psi}_{m,j} + \mu_m \psi_m(x^-_{j+\frac{1}{2}}) - \frac{\Sigma_s}{2}\triangle x\Big(\sum_{n=1}^{m-1} w_n \overline{\widetilde{\psi}}_{n,j} + \sum_{n=m}^{M} w_n \overline{\psi}_{n,j}\Big). \quad (4.3)$$

Since the right-hand side of (4.2) involves only the modified upstream value $\widetilde{\psi}_m(x^-_{j-\frac{1}{2}})$ and the nonnegative source average $\overline{q}_{m,j}$, it follows that

$$LHS(\psi_{m,j}) \geqslant 0.$$

The above construction extends naturally to two spatial dimensions, and the details are omitted for brevity.

Remark. Since the positivity-preserving limiter is designed to maintain the local conservation quantity defined in (4.3), the modified solution $\widetilde{\psi}_m$ and the unmodified solution ψ_m satisfy $LHS(\psi_{m,j}) = LHS(\widetilde{\psi}_{m,j})$. Recalling the definition of $LHS(\cdot)$, this identity yields

$$\Sigma_t \triangle x\, \overline{\psi}_{m,j} + \mu_m \psi_m(x^-_{j+\frac{1}{2}}) - \frac{\Sigma_s}{2}\triangle x w_m \overline{\psi}_{m,j} = \Sigma_t \triangle x\, \overline{\widetilde{\psi}}_{m,j} + \mu_m \widetilde{\psi}_m(x^-_{j+\frac{1}{2}}) - \frac{\Sigma_s}{2}\triangle x w_m \overline{\widetilde{\psi}}_{m,j}. \quad (4.4)$$

Since both $\psi_{m,j}(x)$ and $\widetilde{\psi}_{m,j}(x)$ are polynomials on the cell S_j, their cell averages can be represented by point values. That is, there exist points x_j^b, $\widetilde{x}_j^b \in S_j$ such that

$$\overline{\psi}_{m,j} = \psi_m(x_j^b), \qquad \overline{\widetilde{\psi}}_{m,j} = \widetilde{\psi}_m(\widetilde{x}_j^b).$$

Combining these identities with (4.4), we conclude that there exist points x_j^q, $\widetilde{x}_j^q \in S_j$ such that

$$\psi_m(x_j^q) = \widetilde{\psi}_m(\widetilde{x}_j^q).$$

We now show that the modified solution $\widetilde{\psi}_m$ preserves the conservative structure required for convergence to a weak solution in the sense of the Lax–Wendroff theorem. Let $v \in C_c^\infty(\mathbb{R})$ be a smooth test function. The difference between the discrete weak formulations corresponding to ψ_m and $\widetilde{\psi}_m$ can be expressed as

$$\begin{aligned}
|D_m| &= \left| \sum_j \frac{\Sigma_s}{2} \sum_{n=m}^{M} w_n \big(\overline{\psi}_{n,j} - \overline{\widetilde{\psi}}_{n,j}\big) \triangle x v_x(x_j) \right| \\
&\leq C \triangle x \sum_j \big| \psi_m(x_j^b) - \psi_m(x_j^q) + \widetilde{\psi}_m(\widetilde{x}_j^q) - \widetilde{\psi}_m(\widetilde{x}_j^b) \big| \\
&\leq C \triangle x \Big(\sum_j \big| \psi_m(x_j^b) - \psi_m(x_j^q) \big| + \sum_j \big| \widetilde{\psi}_m(\widetilde{x}_j^q) - \widetilde{\psi}_m(\widetilde{x}_j^b) \big| \Big) \\
&\leq C \triangle x \Big(TV(\psi_m) + TV(\widetilde{\psi}_m) \Big),
\end{aligned}$$

where $TV(\cdot)$ denotes the total variation.

Therefore, provided that both ψ_m and $\widetilde{\psi}_m$ have uniformly bounded total variation, the quantity $|D_m|$ tends to zero as $\triangle x \to 0$. It follows that, if the numerical solution converges with bounded total variation, its limit satisfies the weak formulation of the original transport equation. Consequently, the positivity-preserving limiter that maintains the defined local conservation quantity preserves the conservative structure required for convergence in the sense of the Lax–Wendroff framework.

4.2 Positivity-preserving limiter

In [30], two types of positivity-preserving limiters were developed for stationary hyperbolic equations. It has been shown that limiters constructed to preserve an appropriate local conservation quantity can be designed so that the modification introduced at the downstream boundary does not affect the optimal convergence order of the underlying high-order scheme. In this sense, the resulting numerical approximation retains its high-order accuracy in downstream cells while satisfying the positivity requirement.

Based on the local conservation quantity introduced in the previous subsection, we construct a positivity-preserving limiter for the S_N radiative transfer equations. The proposed

limiter does not rely on the specific quadrature nodes and maintains both positivity and local conservation. For clarity of presentation, the construction is described in one spatial dimension; the extension to two dimensions follows the same principle.

Let $\psi_{m,j}(x)$ denote the DG approximation of the angular flux corresponding to direction m on the cell S_j. The modified solution is defined by

$$\widetilde{\psi}_{m,j}(x) = \theta_j\, \hat{\psi}_{m,j}(x), \qquad \hat{\psi}_{m,j}(x) = \psi_{m,j}(x) + \epsilon_j, \qquad \theta_j = \frac{LHS(\psi_{m,j})}{LHS(\hat{\psi}_{m,j})},$$

where the shift parameter ϵ_j is given by

$$\epsilon_j = -\min\Big\{\min_{x\in K_j} \psi_{m,j}(x),\, 0\Big\}.$$

Here the set $K_j = \{x_{j-\frac{1}{2}}, \hat{x}_1, \ldots, \hat{x}_{q_N}, x_{j+\frac{1}{2}}\}$ consists of the cell endpoints together with the Gauss quadrature points $\{\hat{x}_q\}_{q=1}^{q_N}$ used in the numerical integration. The set K_j denotes the collection of points at which the solution must remain positive. In this work, it is defined to include both endpoints of the cell S_j and the Gauss quadrature points employed in the numerical integration.

From the definition of $\hat{\psi}_{m,j}$, we have $\hat{\psi}_{m,j}(x) \geqslant 0$ for all $x \in K_j$. Moreover, since the local conservation quantity $LHS(\cdot)$ defined in (4.3) depends linearly on $\psi_{m,j}$, it follows that

$$LHS(\hat{\psi}_{m,j}) \geqslant LHS(\psi_{m,j}) \geqslant 0.$$

This implies $\theta_j \in [0, 1]$. Consequently, the modified solution $\widetilde{\psi}_{m,j}(x)$ preserves the local conservation quantity and maintains positivity at all points in K_j.

5 Numerical results

In this section, numerical experiments are conducted for both steady and time-dependent radiative transfer problems to evaluate the performance of the proposed high-order conservative positivity-preserving accelerated DG method. For each test case, we compare standard source iteration, diffusion-accelerated iteration, and their positivity-preserving counterparts

to examine the impact of acceleration and positivity enforcement on accuracy, robustness, and convergence behavior. In all experiments, the source iteration method is terminated based on the criterion defined in Section 2, with $\varepsilon_{\mathrm{SI}} = 10^{-11}$ unless otherwise specified. The angular variable is discretized using standard discrete-ordinate quadrature rules: S_8 quadrature is used for one-dimensional tests, and P_8–T_8 quadrature is employed for two-dimensional tests.

5.1 Accuracy test

Example 1. We first consider the one-dimensional steady radiative transfer equation (2.1) on the spatial domain $[0, 1]$, subject to vacuum boundary conditions at both ends. To examine the convergence behavior and robustness of the accelerated method in an extremely scattering-dominated regime, we choose a very large total cross section $\Sigma_t = 10007000$ and scattering cross section $\Sigma_s = 10000000$, corresponding to a scattering ratio $\Sigma_s/\Sigma_t \approx 0.9993$. For such strongly scattering problems, the classical source iteration method converges extremely slowly and is computationally impractical without acceleration.

The exact solution is given by

$$\psi(x, \mu) = \sin^4(\pi x),$$

and the source term is prescribed as

$$q(x, \mu) = 4\pi\mu \cos(\pi x) \sin^3(\pi x) + \Sigma_a \sin^4(\pi x),$$

which is constructed to be compatible with the exact solution and the positivity requirements of the numerical discretization.

We solve this problem using the classical SI method, the DSA method, and their conservative positivity-preserving formulations. For each method, we report the L^1, L^2, and L^∞ errors, the observed convergence orders, the number of iterations N_{SI} required for convergence, and the total CPU time. In addition, we record the minimum value of the numerical

solution at quadrature points and, for the positivity-preserving schemes, the percentage of cells where the limiter is activated.

Tables 5.1 and 5.2 summarize the numerical results obtained with P^1- and P^2-DG discretizations, respectively. For both polynomial degrees, the diffusion-based acceleration reduces the number of source iterations by up to four orders of magnitude compared with the classical source iteration, while retaining the expected second- and third-order spatial accuracy. This demonstrates the effectiveness of the acceleration strategy in optically thick regimes.

When the conservative positivity-preserving limiter is applied as a postprocessing step to the converged solutions, non-negativity of the radiation intensity is enforced with only one additional iteration. As shown in Tables 5.1 and 5.2, the minimum values of the numerical solutions become non-negative, while the observed convergence orders remain unchanged. This indicates that the proposed limiter effectively eliminates nonphysical negative values without degrading the accuracy of the DG discretization.

Example 2. In the numerical solution of time-dependent radiative transfer problems, an iteratively converged solution is required at each time step, which makes the advantages of accelerated iterative methods particularly pronounced. In this example, we perform an accuracy study for the one-dimensional time-dependent radiative transfer equation (2.4).

To examine both the positivity-preserving property and the acceleration efficiency of the proposed high-order conservative positivity-preserving accelerated iteration method, the coefficients are chosen as $\Sigma_t = 505000$ and $\Sigma_s = 500000$, respectively. With this choice of parameters, the source term is

$$q(x,\mu,t) = e^{-t}\left(-\frac{1}{c}\sin^4(\pi x) + 4\pi\mu\cos(\pi x)\sin^3(\pi x) + \Sigma_a \sin^4(\pi x)\right).$$

The photon speed is set to $c = 3.0 \times 10^8$. The initial condition is given by $\psi(x,\mu,0) = \sin^4(\pi x)$, and vacuum boundary conditions are imposed at both ends of the spatial domain.

Table 5.1: Numerical results for the one-dimensional steady radiative transfer equation obtained on N cell uniform meshes using the P^1-DG discretization. N_{SI} denotes the number of iterations required for convergence.

SI									
N	L^1 error	order	L^2 error	order	L^∞ error	order	$\min u_h$	N_{SI}	CPU(s)
10	4.107E-02		2.052E-02		2.979E-02		-3.07E-03	17144	1.1002
20	1.042E-02	1.978	5.183E-03	1.985	8.026E-03	1.892	-4.20E-04	17126	2.1608
40	2.615E-03	1.995	1.299E-03	1.996	2.044E-03	1.973	-3.00E-05	17121	4.3822
80	6.543E-04	1.999	3.250E-04	1.999	5.133E-04	1.993	-1.90E-06	17120	8.7119
160	1.636E-04	2.000	8.127E-05	2.000	1.285E-04	1.998	-1.15E-07	17120	18.1772
SI-pp									
N	L^1 error	order	L^2 error	order	L^∞ error	order	Limiter(%)	N_{SI}	CPU(s)
10	1.123E-01		7.647E-02		1.184E-01		40.00	17145	1.1546
20	1.294E-02	3.118	6.447E-03	3.568	9.076E-03	3.706	20.00	17127	2.2010
40	2.696E-03	2.263	1.311E-03	2.298	2.044E-03	2.151	10.00	17122	5.0644
80	6.568E-04	2.037	3.251E-04	2.012	5.133E-04	1.993	5.00	17121	10.3477
160	1.637E-04	2.005	8.127E-05	2.000	1.285E-04	1.998	2.50	17121	19.1814
DSA									
N	L^1 error	order	L^2 error	order	L^∞ error	order	$\min u_h$	N_{SI}	CPU(s)
10	4.107E-02		2.052E-02		2.979E-02		-3.07E-03	6	0.0005
20	1.042E-02	1.978	5.183E-03	1.985	8.026E-03	1.892	-4.20E-04	5	0.0007
40	2.615E-03	1.995	1.299E-03	1.996	2.044E-03	1.973	-3.00E-05	5	0.0027
80	6.543E-04	1.999	3.250E-04	1.999	5.133E-04	1.993	-1.90E-06	5	0.0043
160	1.636E-04	2.000	8.127E-05	2.000	1.285E-04	1.998	-1.15E-07	5	0.0091
DSA-pp									
N	L^1 error	order	L^2 error	order	L^∞ error	order	Limiter(%)	N_{SI}	CPU(s)
10	1.123E-01		7.647E-02		1.184E-01		40.00	7	0.0007
20	1.294E-02	3.118	6.447E-03	3.568	9.076E-03	3.706	20.00	6	0.0010
40	2.696E-03	2.263	1.311E-03	2.298	2.044E-03	2.151	10.00	6	0.0033
80	6.568E-04	2.037	3.251E-04	2.012	5.133E-04	1.993	5.00	6	0.0057
160	1.637E-04	2.005	8.127E-05	2.000	1.285E-04	1.998	2.50	6	0.0124

Table 5.2: Numerical results for the one-dimensional steady radiative transfer equation obtained on N cell uniform meshes using the P^2- DG discretization. N_{SI} denotes the number of iterations required for convergence.

SI									
N	L^1 error	order	L^2 error	order	L^∞ error	order	$\min u_h$	N_{SI}	CPU(s)
10	3.758E-03		1.719E-03		2.760E-03		-3.10E-04	17121	1.2764
20	4.540E-04	3.049	2.175E-04	2.983	3.468E-04	2.993	-2.10E-05	17119	2.4599
40	5.642E-05	3.008	2.728E-05	2.995	4.338E-05	2.999	-1.36E-06	17120	5.0286
80	7.110E-06	2.988	3.416E-06	2.998	5.327E-06	3.026	-8.71E-08	17120	10.0791
160	9.017E-07	2.979	4.286E-07	2.995	6.458E-07	3.044	-5.69E-09	17120	19.8884
SI-pp									
N	L^1 error	order	L^2 error	order	L^∞ error	order	Limiter(%)	N_{SI}	CPU(s)
10	6.262E-03		4.216E-03		9.081E-03		20.00	17122	1.4087
20	5.342E-04	3.551	2.805E-04	3.910	5.965E-04	3.928	10.00	17120	2.7039
40	5.894E-05	3.180	2.840E-05	3.304	4.338E-05	3.781	5.00	17121	5.4911
80	7.189E-06	3.035	3.434E-06	3.048	5.327E-06	3.026	2.50	17121	11.1045
160	9.041E-07	2.991	4.289E-07	3.001	6.458E-07	3.044	1.25	17121	22.2421
DSA									
N	L^1 error	order	L^2 error	order	L^∞ error	order	$\min u_h$	N_{SI}	CPU(s)
10	3.758E-03		1.719E-03		2.760E-03		-3.10E-04	6	0.0040
20	4.540E-04	3.049	2.175E-04	2.983	3.468E-04	2.993	-2.10E-05	6	0.0130
40	5.642E-05	3.008	2.728E-05	2.995	4.338E-05	2.999	-1.36E-06	8	0.0115
80	7.110E-06	2.988	3.416E-06	2.998	5.327E-06	3.026	-8.71E-08	6	0.0143
160	9.016E-07	2.979	4.286E-07	2.995	6.453E-07	3.045	-5.69E-09	6	0.0229
DSA-pp									
N	L^1 error	order	L^2 error	order	L^∞ error	order	Limiter(%)	N_{SI}	CPU(s)
10	6.262E-03		4.216E-03		9.081E-03		20.00	7	0.0048
20	5.342E-04	3.551	2.805E-04	3.910	5.965E-04	3.928	10.00	7	0.0137
40	5.894E-05	3.180	2.840E-05	3.304	4.338E-05	3.781	5.00	9	0.0152
80	7.189E-06	3.035	3.434E-06	3.048	5.327E-06	3.026	2.50	7	0.0176
160	9.041E-07	2.991	4.289E-07	3.001	6.453E-07	3.045	1.25	7	0.0284

The exact solution of this problem is

$$\psi(x, \mu, t) = e^{-t} \sin^4(\pi x).$$

The final simulation time is set to $T = 0.1$. The time derivative is discretized using the backward Euler method, which is first-order accurate in time. A small time step $\Delta t = 10^{-3}$ is used so that the temporal discretization error does not dominate the spatial error in the accuracy study. Tables 5.3 and 5.4 summarize the numerical errors and observed convergence orders obtained with the P^1- and P^2-DG discretizations, respectively, confirming the expected second-order and third-order spatial accuracy.

In addition, Tables 5.3 and 5.4 report the average number of iterations required to reach convergence over all time steps for both the source iteration and the DSA methods. A substantial reduction in the number of iterations is observed when DSA is employed. To further assess the effectiveness of the positivity-preserving limiter, we also report the minimum value of the numerical solution at the final time, as well as the percentage of cells in which the limiter is activated. The results indicate that the proposed positivity-preserving limiter enforces non-negativity of the radiation intensity without degrading the high-order accuracy of the DG scheme. Together with the significant reduction in iteration counts achieved by DSA, this demonstrates that the proposed conservative positivity-preserving acceleration framework is both accurate and robust for time-dependent radiative transfer problems in highly scattering and optically thick regimes.

Example 3. We next consider a two-dimensional steady radiative transfer equation (2.5) posed on the spatial domain $[0, 1] \times [0, 1]$. This test is primarily intended to assess the high-order spatial accuracy of the proposed method in a higher-dimensional setting. The total and scattering cross sections are set to $\Sigma_t = 101000$ and $\Sigma_s = 100000$, respectively, placing the problem in a strongly scattering regime. The source term is prescribed as

$$q(x, y, \mu, \lambda) = 4\pi\mu(1 - 2x) \sin^3\big(\pi x(1 - x)\big) \cos\big(\pi x(1 - x)\big) \sin^4\big(\pi y(1 - y)\big)$$
$$+ 4\pi\lambda(1 - 2y) \sin^4\big(\pi x(1 - x)\big) \sin^3\big(\pi y(1 - y)\big) \cos\big(\pi y(1 - y)\big) + \Sigma_a \sin^4\big(\pi x(1 - x)\big) \sin^4\big(\pi y(1 - y)\big),$$

Table 5.3: Numerical results for the one-dimensional unsteady radiative transfer equation obtained on N cell uniform meshes using the P^1-DG discretization. N_{SI} denotes the average number of iterations required to reach convergence over all time.

SI								
N	L^1 error	order	L^2 error	order	L^∞ error	order	$\min u_h$	N_{SI}
10	3.716E-02		1.856E-02		2.697E-02		-2.77E-03	964.54
20	9.431E-03	1.978	4.690E-03	1.985	7.265E-03	1.892	-3.79E-04	963.31
40	2.366E-03	1.995	1.176E-03	1.996	1.850E-03	1.973	-2.70E-05	962.96
80	5.920E-04	1.999	2.941E-04	1.999	4.649E-04	1.993	-1.70E-06	962.86
160	1.480E-04	2.000	7.354E-05	2.000	1.165E-04	1.997	-1.01E-07	962.84
SI-pp								
N	L^1 error	order	L^2 error	order	L^∞ error	order	Limiter(%)	N_{SI}
10	9.308E-02		6.180E-02		9.734E-02		40.41	1218.58
20	1.150E-02	3.017	5.681E-03	3.443	7.741E-03	3.652	20.28	1071.33
40	2.433E-03	2.241	1.185E-03	2.261	1.850E-03	2.065	10.68	963.96
80	5.941E-04	2.034	2.942E-04	2.010	4.649E-04	1.993	5.40	963.86
160	1.481E-04	2.004	7.354E-05	2.000	1.165E-04	1.997	2.76	963.84
DSA								
N	L^1 error	order	L^2 error	order	L^∞ error	order	$\min u_h$	N_{SI}
10	3.716E-02		1.856E-02		2.697E-02		-2.77E-03	5.01
20	9.431E-03	1.978	4.690E-03	1.985	7.265E-03	1.892	-3.79E-04	4.02
40	2.366E-03	1.995	1.176E-03	1.996	1.850E-03	1.973	-2.70E-05	4.01
80	5.920E-04	1.999	2.941E-04	1.999	4.649E-04	1.993	-1.70E-06	4.01
160	1.480E-04	2.000	7.354E-05	2.000	1.165E-04	1.997	-1.01E-07	4.01
DSA-pp								
N	L^1 error	order	L^2 error	order	L^∞ error	order	Limiter(%)	N_{SI}
10	9.308E-02		6.180E-02		9.734E-02		40.50	7.99
20	1.150E-02	3.017	5.681E-03	3.443	7.741E-03	3.652	20.28	7.99
40	2.433E-03	2.241	1.185E-03	2.261	1.850E-03	2.065	10.71	7.98
80	5.941E-04	2.034	2.942E-04	2.010	4.649E-04	1.993	5.39	7.98
160	1.481E-04	2.004	7.354E-05	2.000	1.165E-04	1.997	2.75	7.98

Table 5.4: Numerical results for the one-dimensional unsteady radiative transfer equation obtained on N cell uniform meshes using the P^2-DG discretization. N_{SI} denotes the average number of iterations required to reach convergence over all time.

SI								
N	L^1 error	order	L^2 error	order	L^∞ error	order	$\min u_h$	N_{SI}
10	3.403E-03		1.556E-03		2.494E-03		-2.81E-04	962.92
20	4.115E-04	3.048	1.968E-04	2.983	3.127E-04	2.995	-1.91E-05	962.85
40	5.122E-05	3.006	2.469E-05	2.995	3.900E-05	3.003	-1.24E-06	962.83
80	6.475E-06	2.984	3.094E-06	2.996	4.757E-06	3.035	-8.03E-08	962.83
160	8.256E-07	2.971	3.894E-07	2.990	5.711E-07	3.058	-5.33E-09	962.85
SI-pp								
N	L^1 error	order	L^2 error	order	L^∞ error	order	Limiter(%)	N_{SI}
10	5.498E-03		3.616E-03		7.800E-03		20.00	1075.06
20	4.788E-04	3.521	2.478E-04	3.867	5.136E-04	3.925	10.00	963.84
40	5.334E-05	3.166	2.559E-05	3.275	3.900E-05	3.719	5.00	963.86
80	6.541E-06	3.028	3.109E-06	3.041	4.757E-06	3.035	2.50	963.83
160	8.276E-07	2.982	3.897E-07	2.996	5.711E-07	3.058	1.25	963.84
DSA								
N	L^1 error	order	L^2 error	order	L^∞ error	order	$\min u_h$	N_{SI}
10	3.403E-03		1.556E-03		2.494E-03		-2.81E-04	5.01
20	4.115E-04	3.048	1.968E-04	2.983	3.127E-04	2.995	-1.91E-05	5.01
40	5.122E-05	3.006	2.469E-05	2.995	3.900E-05	3.003	-1.24E-06	5.01
80	6.475E-06	2.984	3.094E-06	2.996	4.757E-06	3.035	-8.03E-08	4.41
160	8.256E-07	2.971	3.894E-07	2.990	5.711E-07	3.058	-5.33E-09	4.02
DSA-pp								
N	L^1 error	order	L^2 error	order	L^∞ error	order	Limiter(%)	N_{SI}
10	5.498E-03		3.616E-03		7.800E-03		20.00	7.99
20	4.788E-04	3.521	2.478E-04	3.867	5.136E-04	3.925	10.00	7.99
40	5.334E-05	3.166	2.559E-05	3.275	3.900E-05	3.719	5.00	7.99
80	6.541E-06	3.028	3.109E-06	3.041	4.757E-06	3.035	2.50	8.98
160	8.276E-07	2.982	3.897E-07	2.996	5.711E-07	3.058	1.25	8.98

The corresponding exact solution is given by

$$\psi(x, y, \mu, \lambda) = \sin^4(\pi x(1-x)) \sin^4(\pi y(1-y)).$$

The numerical results for the two-dimensional steady radiative transfer problem, computed with the Q^1- and P^2-DG discretizations, are summarized in Tables 5.5 and 5.6, respectively. In both cases, the designed high-order accuracy is observed, even in the strongly scattering regime with $\Sigma_s/\Sigma_t \approx 0.99$. For this two-dimensional problem, the classical source iteration requires more than 800 iterations to converge on all tested meshes, rendering the unaccelerated solver computationally impractical. With diffusion synthetic acceleration, the iteration counts are significantly reduced for both discretizations. In particular, for the Q^1-DG scheme, the number of iterations remains stable at approximately six for all mesh resolutions, whereas for the P^2-DG scheme, the iteration counts are not strictly constant but remain on the order of ten. These results show that the acceleration strategy is effective for different polynomial representations in two dimensions. In the absence of the conservative positivity-preserving limiter, small negative values of the radiation intensity are observed, whereas non-negativity is preserved when the limiter is applied, with the high-order accuracy remaining unchanged.

Example 4. Finally, we consider a two-dimensional unsteady radiative transfer equation (2.7) posed on the spatial domain $[0, 1] \times [0, 1]$ with vacuum boundary conditions. The total and scattering cross sections are taken as $\Sigma_t = 101000$ and $\Sigma_s = 100000$, respectively, corresponding to a strongly scattering regime. The source term is chosen consistently so that the exact solution is given by

$$\psi(x, y, \mu, \lambda, t) = e^{-t} \sin^4\big(\pi x(1-x)\big) \sin^4\big(\pi y(1-y)\big).$$

The final simulation time is set to $T = 0.1$. In this two-dimensional time-dependent setting, only the numerical results obtained with the accelerated schemes, with and without the positivity-preserving limiter, are reported, as the classical source iteration is computationally impractical due to the high iteration counts.

Table 5.5: Numerical results for the two-dimensional steady radiative transfer equation obtained on uniform $N \times N$ rectangular meshes using the Q^1-DG discretization. N_{SI} denotes the number of iterations required for convergence.

SI									
N	L^1 error	order	L^2 error	order	L^∞ error	order	$\min u_h$	N_{SI}	CPU(s)
10	1.807E-02		3.551E-03		2.548E-03		-3.12E-04	840	19.3266
20	4.511E-03	2.002	9.008E-04	1.979	6.510E-04	1.969	-4.13E-05	838	72.8491
40	1.128E-03	1.999	2.259E-04	1.996	1.636E-04	1.992	-5.25E-06	838	325.4949
60	5.018E-04	1.999	1.005E-04	1.999	7.284E-05	1.996	-1.18E-06	838	802.6643
80	2.823E-04	2.000	5.652E-05	1.999	4.101E-05	1.997	-3.83E-07	838	1425.9968
SI-pp									
N	L^1 error	order	L^2 error	order	L^∞ error	order	Limiter(%)	N_{SI}	CPU(s)
10	2.021E-02		3.977E-03		2.548E-03		36.00	841	35.8579
20	6.359E-03	1.668	1.444E-03	1.462	1.334E-03	0.933	27.75	839	148.2742
40	1.202E-03	2.404	2.354E-04	2.617	1.636E-04	3.027	14.44	839	667.3187
60	5.120E-04	2.104	1.011E-04	2.084	7.284E-05	1.996	9.75	839	1232.6560
80	2.848E-04	2.039	5.661E-05	2.016	4.101E-05	1.997	7.36	839	1608.6240
DSA									
N	L^1 error	order	L^2 error	order	L^∞ error	order	$\min u_h$	N_{SI}	CPU(s)
10	1.807E-02		3.551E-03		2.548E-03		-3.12E-04	6	0.1792
20	4.511E-03	2.002	9.008E-04	1.979	6.510E-04	1.969	-4.13E-05	6	0.7110
40	1.128E-03	1.999	2.259E-04	1.996	1.637E-04	1.992	-5.25E-06	6	3.3377
60	5.018E-04	1.998	1.005E-04	1.999	7.285E-05	1.996	-1.18E-06	6	9.8500
80	2.823E-04	2.000	5.652E-05	1.999	4.102E-05	1.996	-3.83E-07	6	31.6162
DSA-pp									
N	L^1 error	order	L^2 error	order	L^∞ error	order	Limiter(%)	N_{SI}	CPU(s)
10	2.021E-02		3.977E-03		2.548E-03		36.00	7	0.1923
20	6.359E-03	1.668	1.444E-03	1.462	1.334E-03	0.933	27.75	7	0.8392
40	1.202E-03	2.404	2.354E-04	2.617	1.637E-04	3.027	14.44	7	3.7538
60	5.121E-04	2.104	1.011E-04	2.084	7.285E-05	1.996	9.75	7	10.5057
80	2.848E-04	2.039	5.661E-05	2.016	4.102E-05	1.996	7.36	7	33.2268

Table 5.6: Numerical results for the two-dimensional steady radiative transfer equation obtained on uniform $N \times N$ rectangular meshes using the P^2-DG discretization. N_{SI} denotes the number of iterations required for convergence.

SI									
N	L^1 error	order	L^2 error	order	L^∞ error	order	$\min u_h$	N_{SI}	CPU(s)
10	3.209E-03		6.137E-04		3.500E-04		-4.74E-05	838	27.5053
20	4.002E-04	3.003	7.736E-05	2.988	4.489E-05	2.963	-3.74E-06	838	103.5087
40	4.989E-05	3.004	9.611E-06	3.009	5.569E-06	3.011	-2.81E-07	838	421.0192
60	1.475E-05	3.006	2.823E-06	3.021	1.628E-06	3.034	-6.15E-08	838	973.4260
80	6.213E-06	3.005	1.182E-06	3.027	6.763E-07	3.053	-2.11E-08	838	1723.4669
SI-pp									
N	L^1 error	order	L^2 error	order	L^∞ error	order	Limiter(%)	N_{SI}	CPU(s)
10	6.532E-03		1.815E-03		1.302E-03		35.88	839	30.8001
20	5.121E-04	3.673	1.151E-04	3.980	9.464E-05	3.782	18.86	839	122.5725
40	5.330E-05	3.264	1.034E-05	3.476	5.932E-06	3.996	9.66	839	540.7188
60	1.521E-05	3.093	2.895E-06	3.141	1.628E-06	3.189	6.49	839	1130.6054
80	6.326E-06	3.048	1.196E-06	3.072	6.763E-07	3.053	4.88	839	1950.7226
DSA									
N	L^1 error	order	L^2 error	order	L^∞ error	order	$\min u_h$	N_{SI}	CPU(s)
10	3.209E-03		6.137E-04		3.500E-04		-4.74E-05	8	0.3192
20	4.002E-04	3.003	7.736E-05	2.988	4.489E-05	2.963	-3.74E-06	9	1.4287
40	4.989E-05	3.004	9.611E-06	3.009	5.573E-06	3.010	-2.81E-07	10	7.5549
60	1.475E-05	3.006	2.824E-06	3.021	1.631E-06	3.030	-6.15E-08	11	24.3500
80	6.212E-06	3.005	1.182E-06	3.027	6.796E-07	3.043	-2.11E-08	12	72.5383
DSA-pp									
N	L^1 error	order	L^2 error	order	L^∞ error	order	Limiter(%)	N_{SI}	CPU(s)
10	6.532E-03		1.815E-03		1.302E-03		35.88	9	0.3944
20	5.121E-04	3.673	1.151E-04	3.980	9.464E-05	3.782	18.86	10	1.7411
40	5.330E-05	3.264	1.034E-05	3.476	5.932E-06	3.996	9.66	11	8.1698
60	1.521E-05	3.093	2.895E-06	3.141	1.631E-06	3.184	6.49	12	25.9325
80	6.326E-06	3.049	1.196E-06	3.072	6.796E-07	3.043	4.88	13	75.2146

Tables 5.7 and 5.8 present the numerical results for the Q^1- and P^2-DG discretizations, respectively. In both cases, the accelerated schemes attain the designed high-order spatial accuracy. The conservative positivity-preserving limiter maintains non-negativity of the numerical solution and preserves the high-order accuracy.

Table 5.7: Numerical results for the two-dimensional unsteady radiative transfer equation obtained on uniform $N \times N$ rectangular meshes using the Q^1-DG discretization. N_{SI} denotes the average number of iterations required to reach convergence over all time.

DSA								
N	L^1 error	order	L^2 error	order	L^∞ error	order	$\min u_h$	N_{SI}
10	1.637E-02		3.214E-03		2.302E-03		-2.87E-04	4.01
20	4.086E-03	2.002	8.151E-04	1.979	5.883E-04	1.968	-3.98E-05	4.01
40	1.021E-03	2.000	2.044E-04	1.995	1.479E-04	1.992	-5.29E-06	3.02
60	4.542E-04	1.998	9.094E-05	1.998	6.585E-05	1.995	-1.24E-06	3.02
80	2.557E-04	1.997	5.122E-05	1.995	3.714E-05	1.991	-4.24E-07	3.02
DSA-pp								
N	L^1 error	order	L^2 error	order	L^∞ error	order	Limiter(%)	N_{SI}
10	1.823E-02		3.588E-03		2.302E-03		36.00	6.99
20	5.555E-03	1.714	1.227E-03	1.548	1.096E-03	1.070	27.75	6.99
40	1.082E-03	2.360	2.119E-04	2.534	1.479E-04	2.890	14.44	6.99
60	4.628E-04	2.095	9.147E-05	2.072	6.585E-05	1.995	9.75	6.99
80	2.578E-04	2.034	5.130E-05	2.010	3.714E-05	1.991	7.36	6.99

5.2 Positivity-preserving test

Example 5. In this test, we consider a one-dimensional steady radiative transfer problem with a discontinuous solution over the domain $[0, 1]$. To construct a strongly scattering regime, the total and scattering cross sections are chosen as $\Sigma_t = 10000$ and $\Sigma_s = 9990$. A piecewise constant solution is prescribed, and the source term is chosen accordingly:

$$\psi(x,\mu) = \begin{cases} 100, & 0.25 < x < 0.75, \\ 0, & \text{otherwise}, \end{cases} \qquad q(x,\mu) = \begin{cases} 1000, & 0.25 < x < 0.75, \\ 0, & \text{otherwise}. \end{cases}$$

Numerical experiments are conducted on a uniform mesh with 60 cells for all four methods. Figure 1 shows the numerical solutions of the radiation intensity along the angular direction

Table 5.8: Numerical results for the two-dimensional unsteady radiative transfer equation obtained on uniform $N \times N$ rectangular meshes using the P^2-DG discretization. N_{SI} denotes the average number of iterations required to reach convergence over all time.

DSA								
N	L^1 error	order	L^2 error	order	L^∞ error	order	$\min u_h$	N_{SI}
10	2.908E-03		5.585E-04		3.174E-04		-4.20E-05	4.02
20	3.639E-04	2.998	7.082E-05	2.979	4.123E-05	2.944	-3.20E-06	4.02
40	4.552E-05	2.999	8.892E-06	2.994	5.151E-06	3.001	-2.25E-07	4.02
60	1.356E-05	2.987	2.645E-06	2.991	1.572E-06	2.926	-4.66E-08	4.02
80	6.106E-06	2.773	1.162E-06	2.860	7.308E-07	2.664	-1.52E-08	4.02
DSA-pp								
N	L^1 error	order	L^2 error	order	L^∞ error	order	Limiter(%)	N_{SI}
10	5.538E-03		1.476E-03		1.054E-03		5.103	7.00
20	4.423E-04	3.646	9.422E-05	3.969	7.260E-05	3.860	2.675	7.00
40	4.742E-05	3.221	9.202E-06	3.356	5.151E-06	3.817	1.366	7.00
60	1.376E-05	3.051	2.666E-06	3.056	1.572E-06	2.926	0.917	7.00
80	6.147E-06	2.801	1.165E-06	2.879	7.308E-07	2.664	0.782	6.19

$\mu = 0.5255$ on a uniform mesh with $N = 60$. The results are obtained using the P^1-DG method and the P^2-DG method. In both cases, the positivity-preserving limiter successfully prevents the appearance of negative radiation intensities for both the classical source iteration and the DSA method, thereby maintaining the physical admissibility of the numerical solution.

We further compare the iteration counts required by different solvers. For the P^1-DG discretization, the classical source iteration requires 12582 iterations to converge, whereas the DSA method converges within 18 iterations. A similar behavior is observed for the P^2-DG discretization, for which the source iteration requires 12576 iterations, while the DSA method again converges in 18 iterations. When the positivity-preserving limiter is applied, only one additional iteration is required in both cases. These results demonstrate that the DSA method, combined with the positivity-preserving limiter, provides an efficient and robust approach for solving radiative transfer problems with discontinuous solutions in strongly scattering regimes.

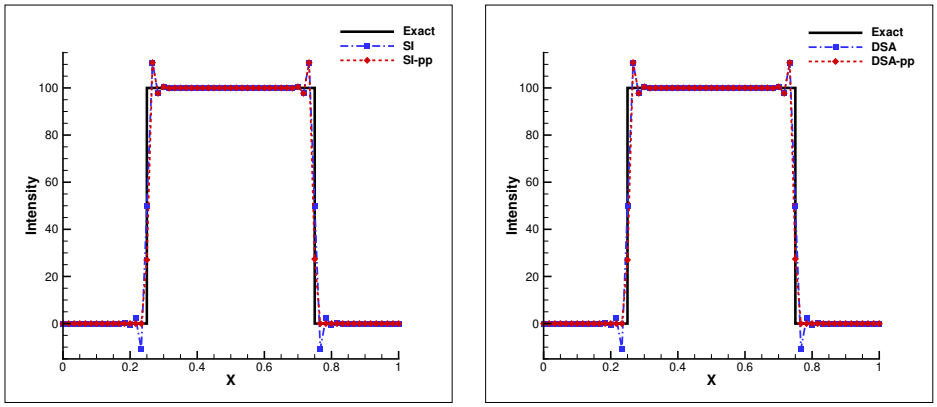

(a) SI, P^1

(b) DSA, P^1

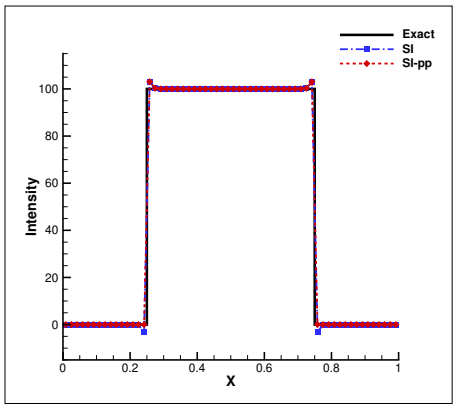

(c) SI, P^2

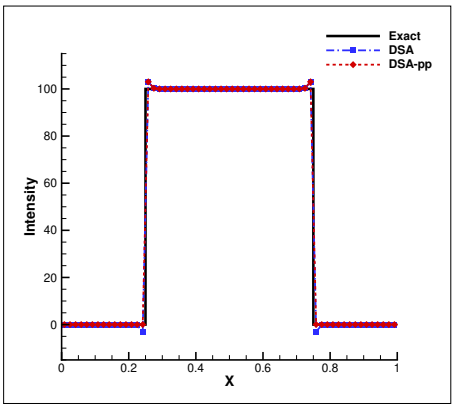

(d) DSA, P^2

Figure 1: Radiative intensity profiles for Example 5 computed using the classical source iteration and diffusion synthetic acceleration. The results obtained with the P^1-DG discretization are shown in (a)–(b), and those obtained with the P^2-DG discretization are shown in (c)–(d). In each subfigure, the numerical solutions with and without the positivity-preserving limiter are displayed for comparison.

Example 6. We next consider a smooth test problem for the one-dimensional steady radiative transfer equation on the spatial domain $[0, 1]$. The solution is constructed to be continuous but highly localized, featuring two sharp Gaussian peaks embedded in a smooth polynomial envelope. Such a configuration provides a stringent test for high-order DG schemes in the presence of strong spatial gradients. The total and scattering cross sections are chosen as $\Sigma_t = 40000$ and $\Sigma_s = 39000$, corresponding to a strongly scattering regime with $\Sigma_s/\Sigma_t = 0.975$. The exact solution is defined as

$$\psi(x, \mu) = x^2(1 - x^2)\left(100e^{-3000(x-0.35)^2} + 120e^{-4000(x-0.65)^2}\right).$$

The source term is then determined analytically so that the above function satisfies the steady radiative transfer equation under vacuum boundary conditions.

The numerical results for this smooth test problem, shown in Figures 2 and 3, are obtained using both the P^1-DG and P^2-DG discretizations on a uniform mesh with 55 cells. Compared with the classical source iteration, the accelerated method reduces the number of transport iterations from 546 to 12, leading to a marked reduction in computational cost.

Small negative values of the radiative intensity are observed in the numerical solutions when no positivity-preserving correction is applied, as indicated by the reported minimum values in the zoomed-in plots. After incorporating the conservative positivity-preserving limiter, the numerical solution remains non-negative, and the overall accuracy of the DG discretization is preserved.

Example 7. We next consider a two-dimensional steady radiative transfer problem with a discontinuous manufactured solution. The spatial domain is $[0, 1] \times [0, 1]$, and vacuum boundary conditions are imposed on the entire boundary. The total and scattering cross sections are set to $\Sigma_t = 10000$ and $\Sigma_s = 9800$, corresponding to a strongly scattering regime. A discontinuous solution is prescribed as a piecewise-constant function supported

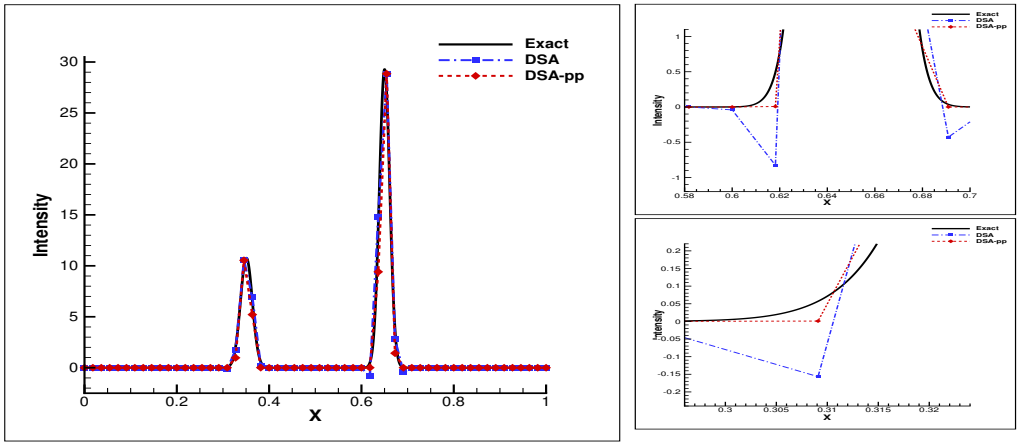

Figure 2: Radiative intensity profiles for Example 6 obtained with the P^1-DG discretization on a uniform mesh with 55 cells using DSA method, with and without the positivity-preserving limiter. The right panels show zoomed-in views of the solution in the regions where small negative values occur.

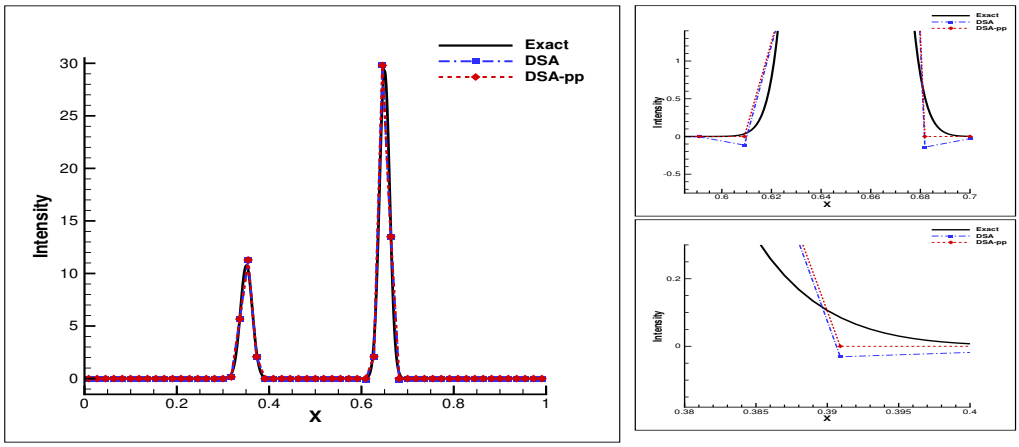

Figure 3: Radiative intensity profiles for Example 6 obtained with the P^2-DG discretization on a uniform mesh with 55 cells using DSA method, with and without the positivity-preserving limiter. The right panels show zoomed-in views of the solution in the regions where small negative values occur.

on a circular region centered at (0.5,0.5), given by

$$\psi(x, y, \mu, \lambda) = \begin{cases} 100, & (x-0.5)^2 + (y-0.5)^2 \leq 0.25^2, \\ 0, & \text{otherwise.} \end{cases}$$

Numerical results are obtained on a uniform 60×60 mesh using the Q^1-DG and P^2-DG discretizations, both with and without the positivity-preserving limiter, as shown in Figure 4. For the Q^1-DG scheme, the accelerated solver converges in 31 iterations, and in 32 iterations when the positivity-preserving limiter is included; by comparison, the unaccelerated source iteration requires 623 iterations. For the P^2-DG scheme, the DSA method reduces the iteration count to 46 iterations, with only one additional iteration required when the positivity-preserving limiter is applied.

Subfigures (c)–(d) in Figure 4 highlight the cells where the positivity-preserving limiter is activated, which are marked by white triangles. The radiative intensity profiles along the diagonal cut line $x = y$ further illustrate the effect of the positivity-preserving correction. Without the positivity-preserving limiter, high-order DG discretizations develop pronounced oscillations in the vicinity of the discontinuity, resulting in severe negative undershoots. The application of the limiter eliminates these nonphysical values while preserving the overall solution structure.

Example 8. We finally consider a classical lattice test problem for the steady radiative transfer equation on the square domain $D = (0, 7) \times (0, 7)$, where the material coefficients are piecewise constant and arranged in a checkerboard pattern. The absorption and scattering cross sections vary according to the lattice structure. The absorption coefficient Σ_a is set to 50 in the black regions shown in Figure 5, and to 0 elsewhere, while the scattering coefficient Σ_s is set to 10 in the gray and white regions and to 0 in the black regions. The source term is defined as $q(x, \mu) = 1$ in the white regions and $q(x, \mu) = 0$ elsewhere. This configuration constitutes a challenging, non-smooth benchmark problem featuring sharp material discontinuities and localized sources, rigorously testing the performance of iterative solvers and positivity-preserving discretizations.

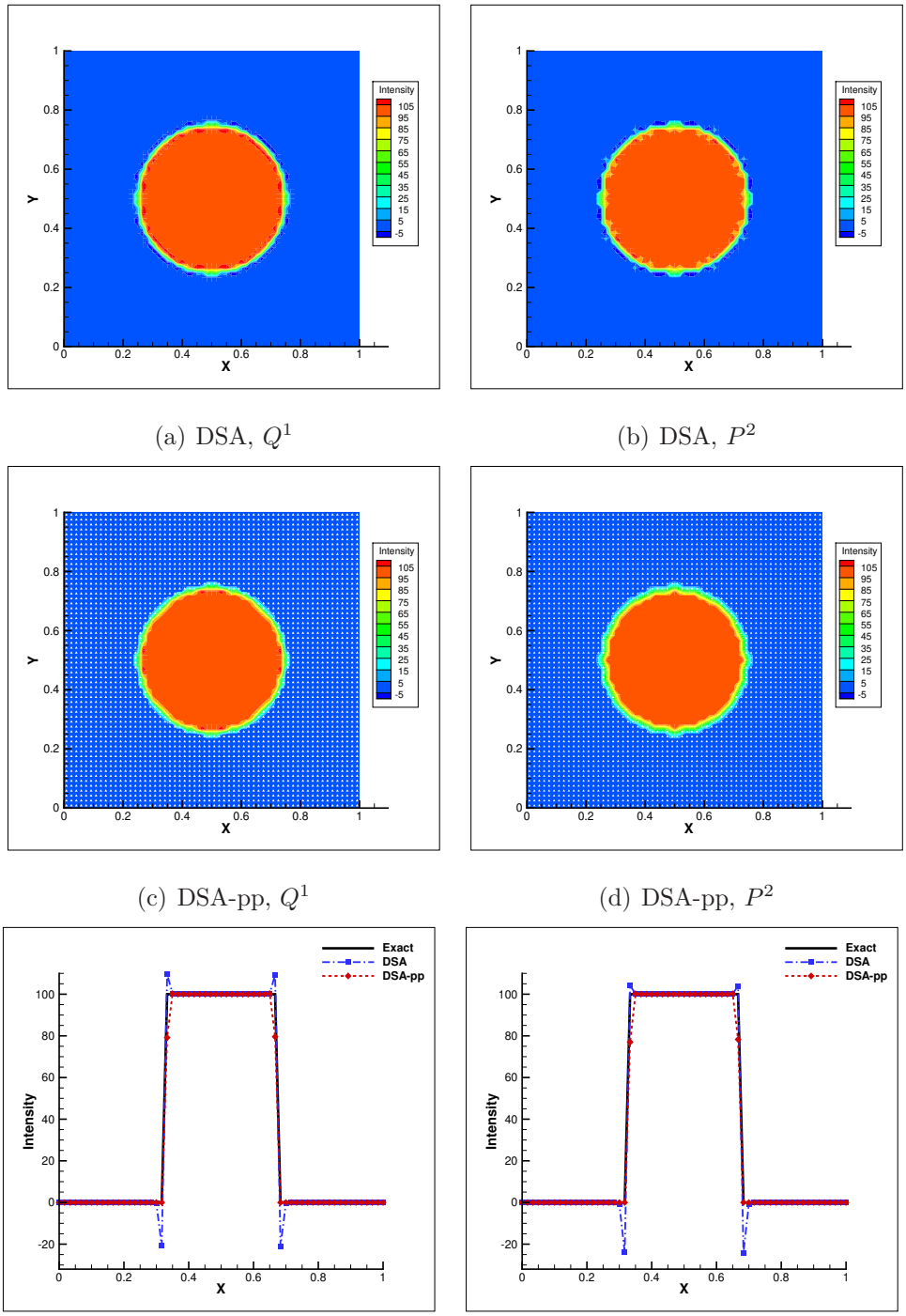

(a) DSA, Q^1

(b) DSA, P^2

(c) DSA-pp, Q^1

(d) DSA-pp, P^2

(e) DSA, Q^1, cut line

(f) DSA, P^2, cut line

Figure 4: Numerical results for the two-dimensional steady radiative transfer problem (Example 7) with a discontinuous manufactured solution on a 60×60 uniform mesh. Panels (a)–(d) show the contours of the radiative intensity computed using DSA method with the Q^1-DG and P^2-DG discretizations, with and without the positivity-preserving limiter. Panels (e)–(f) display the radiative intensity profiles along the diagonal cut line $x = y$.

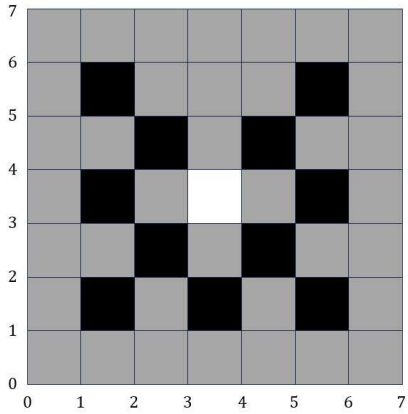

Figure 5: Description of the lattice problem.

The numerical results for the two-dimensional lattice problem are obtained using both the Q^1-DG and P^2-DG discretizations on a 70×70 uniform mesh, as shown in Figure 6. For this highly heterogeneous configuration, the classical source iteration converges slowly, requiring 971 iterations for the Q^1-DG discretization and 973 iterations for the P^2-DG discretization. When diffusion synthetic acceleration is applied, the number of iterations is reduced to 29 and 30, respectively, demonstrating the effectiveness of the acceleration strategy for problems with strongly varying material properties.

The contours of the angularly averaged radiative intensity are plotted on a $\log_{10}$ scale, clearly illustrating the wide range of magnitudes of the radiative intensity present in this lattice problem. When the conservative positivity-preserving limiter is incorporated, the numerical solutions remain non-negative throughout the computational domain. The cells where the limiter is activated are mainly concentrated in the black regions, which correspond to sharp jumps in absorption and scattering coefficients, as shown in the right subfigures. These results indicate that the proposed positivity-preserving correction effectively maintains physical admissibility in strongly non-smooth media.

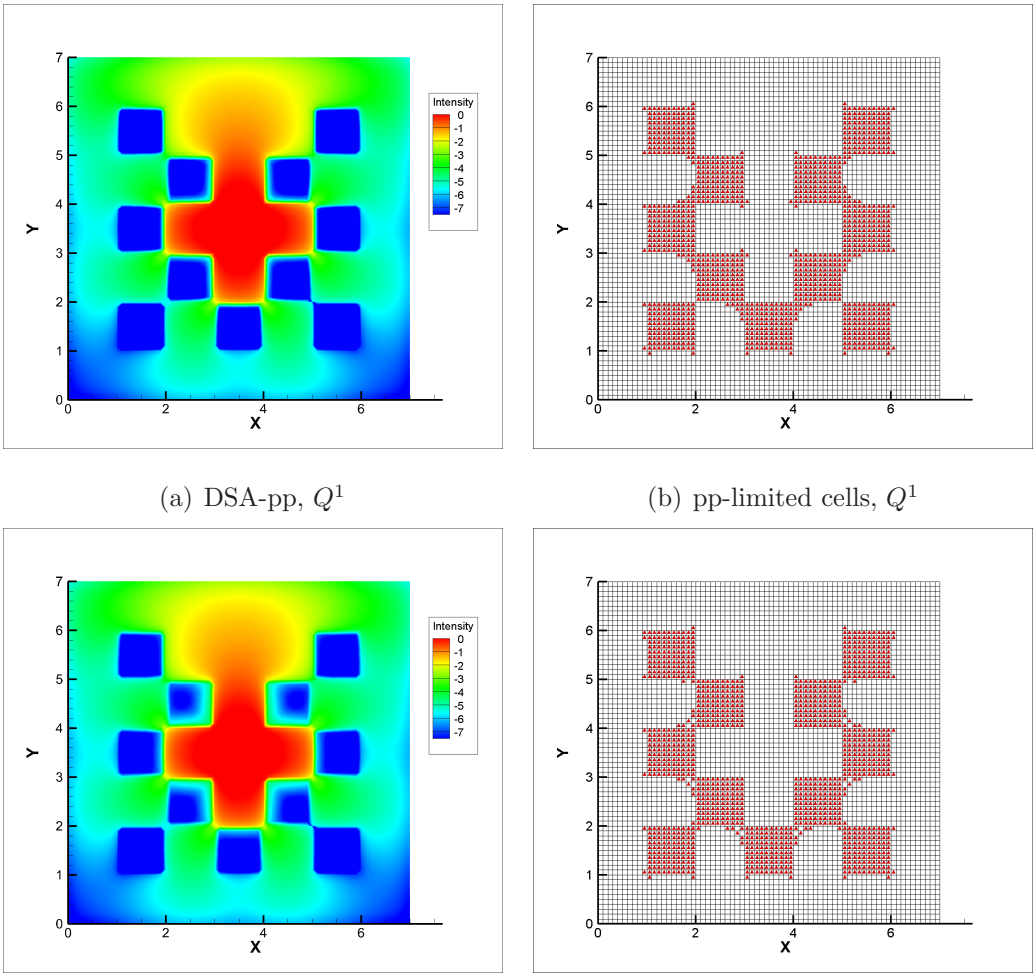

(a) DSA-pp, Q^1

(b) pp-limited cells, Q^1

(c) DSA-pp, P^2

(d) pp-limited cells, P^2

Figure 6: Numerical results for the two-dimensional lattice problem (Example 8) on a 70×70 uniform mesh. Left: contours of the angularly averaged radiative intensity in $\log_{10}$ scale obtained with DSA method using the Q^1-DG and P^2-DG discretizations. Right: cells where the positivity-preserving limiter is activated, marked by red triangular symbols.

6 Concluding remarks

In this work, we have developed a high-order discontinuous Galerkin framework for the S_N radiative transfer equations in which positivity preservation and conservation are incorporated into an accelerated iterative formulation. The proposed framework combines a high-order DG discretization of the S_N radiative transfer equations with a DSA operator that is asymptotically consistent with the discrete diffusion limit of the transport discretization. This diffusion correction is then incorporated into the high-order DG transport unknowns using a moment-based P_1 update procedure. Together, these components promote stable and effective acceleration in optically thick and strongly scattering regimes. Within this accelerated framework, a key contribution is the construction of the high-order conservative positivity-preserving strategy based on suitably defined locally conservative quantities. This design enables the enforcement of non-negativity in the converged radiation intensity while maintaining the conservation structure induced by the DG discretization and retaining high-order accuracy. Numerical results in one and two spatial dimensions, for both steady-state and time-dependent problems, demonstrate that the accelerated iteration converges rapidly in scattering-dominated regimes and that the proposed positivity-preserving mechanism yields physically admissible solutions without compromising accuracy, with substantial reductions in iteration counts compared to unaccelerated source iteration. Future work will focus on extending the present conservative, positivity-preserving accelerated framework to more general spatial discretizations, heterogeneous media, and more complex scattering models.

References

[1] M. L. Adams and E. W. Larsen, *Fast iterative methods for discrete-ordinates particle transport calculations*, Progress in Nuclear Energy, 40(1), 2002, 3-159.

[2] R. E. Alcouffe, *Diffusion synthetic acceleration methods for the diamond-difference discretization of the transport equation*, Nuclear Science and Engineering, 64(2), 1977,

344-355.

[3] D. E. Bruss, J. E. Morel and J. C. Ragusa, *S_2SA preconditioning for the S_n equations with strictly nonnegative spatial discretization*, Journal of Computational Physics, 273, 2014, 706-719.

[4] B. G. Carlson, *Solution of the transport equation by S_n approximations*, Los Alamos: Los Alamos Scientific Laboratory, 1955.

[5] B. Cockburn and C.-W. Shu, *Runge—Kutta discontinuous Galerkin methods for convection-dominated problems*, Journal of Scientific Computing, 16, 2001, 173-261.

[6] J.A. Fleck and J.D. Cummings, *An implicit Monte Carlo scheme for calculating time and frequency dependent nonlinear radiation transport*, Journal of Computational Physics, 8(3), 1971, 313-342.

[7] N.A. Gentile, *Implicit Monte Carlo diffusion—an acceleration method for Monte Carlo time-dependent radiative transfer simulations*, Journal of Computational Physics, 172(2), 2001, 543-571.

[8] J. Guermond and G. Kanschat, *Asymptotic analysis of upwind discontinuous Galerkin approximation of the radiative transport equation in the diffusive limit*, SIAM Journal on Numerical Analysis, 48(1), 2010, 53-78.

[9] T. S. Haut, B. S. Southworth, P. G. Maginot and V. Z. Tomov, *Diffusion synthetic acceleration preconditioning for discontinuous Galerkin discretizations of S_N transport on high-order curved meshes*, SIAM Journal on Scientific Computing, 42(5), 2020, B1271-B1301.

[10] A. D. Kim and A. Ishimaru, *A Chebyshev spectral method for radiative transfer equations applied to electromagnetic wave propagation and scattering in a discrete random medium*, Journal of Computational Physics, 152, 1999, 264-280.

[11] E. W. Larsen, *Unconditionally stable diffusion-synthetic acceleration methods for the slab geometry discrete ordinates equations. Part I: Theory*, Nuclear Science and Engineering, 82(1), 1982, 47-63.

[12] E. W. Larsen, *The asymptotic diffusion limit of discretized transport problems*, Nuclear Science and Engineering, 112(4), 1992, 336-346.

[13] E. W. Larsen and R. E. Alcouffe, *The linear characteristic method for spatially discretizing the discrete-ordinates equations in (x,y)-geometry*, in Proceedings of the ANS/ENS Joint Topical Meeting, Mathematical Methods in Nuclear Engineering, Munich, FRG, 1981.

[14] K. D. Lathrop, *Spatial differencing of the transport equation: Positivity vs. accuracy*, Journal of Computational Physics, 4, 1969, 475-498.

[15] K. D. Lathrop and B. G. Carlson, *Discrete ordinates angular quadrature of the neutron transport equation*, Los Alamos: Los Alamos Scientific Laboratory, 1965.

[16] E. E. Lewis and W. F. Miller, Jr., *Computational Methods of Neutron Transport*, Wiley-Interscience, New York, 1984.

[17] D. Ling, J. Cheng and C.-W. Shu, *Conservative high order positivity-preserving discontinuous Galerkin methods for linear hyperbolic and radiative transfer equations*, Journal of Scientific Computing, 77, 2018, 1801-1831.

[18] P. G. Maginot, J. E. Morel and J. C. Ragusa, *A non-negative moment-preserving spatial discretization scheme for the linearized Boltzmann transport equation in 1-D and 2-D Cartesian geometries*, Journal of Computational Physics, 231, 2012, 6801–6826.

[19] G. L. Olson, *Second-order time evolution of P_N equations for radiation transport*, Journal of Computational Physics, 228(8), 2009, 3072-3083.

[20] G. D. Raithby and E. H. Chui, *A finite-volume method for predicting a radiant heat transfer in enclosures with participating media*, Journal of Heat Transfer, 112(2), 1990, 415-423.

[21] M. M. Razzaque, D. E. Klein and J. R. Howell, *Finite element solution of radiative heat transfer in a two-dimensional rectangular enclosure with gray participating media*, Journal of Heat Transfer, 105(4), 1983, 933-936.

[22] W. H. Reed and T. R. Hill, *Triangular mesh methods for the neutron transport equation*, Tech. Report LA-UR-73-479, Los Alamos Scientific Laboratory, 1973.

[23] Y. Wang and J. C. Ragusa, *A high-order discontinuous Galerkin method for the S_N transport equations on 2D unstructured triangular meshes*, Annals of Nuclear Energy, 36(7), 2009, 931-939.

[24] Y. Wang and J. C. Ragusa, *Diffusion synthetic acceleration for high-order discontinuous finite element S_n transport schemes and application to locally refined unstructured meshes*, Nuclear Science and Engineering, 166(2), 2010, 145-166.

[25] T. A. Wareing, *Asymptotic diffusion accelerated discontinuous finite element methods for transport problems*, PhD thesis, United States: The University of Michigan, 1991.

[26] T. A. Wareing, *An exponential discontinuous scheme for discrete-ordinate calculations in Cartesian geometries*, in Proceedings of the Joint International Conference on Mathematical Methods and Supercomputing for Nuclear Applications, Saratoga Springs, NY, 1997.

[27] J. S. Warsa, T. A. Wareing and J. E. Morel, *Fully consistent diffusion synthetic acceleration of linear discontinuous S_n transport discretizations on unstructured tetrahedral meshes*, Nuclear Science and Engineering, 141(3), 2002, 236-251.

[28] J. S. Warsa, T. A. Wareing and J. E. Morel, *Solution of the discontinuous P1 equations in two-dimensional Cartesian geometry with two-level preconditioning*, SIAM Journal on Scientific Computing, 24(6), 2003, 2093-2124.

[29] B. Wendroff, *A difference scheme for radiative transfer*, Journal of Computational Physics, 4(2), 1969, 211-229.

[30] Z. Xu and C.-W. Shu, *On the conservation property of positivity-preserving discontinuous Galerkin methods for stationary hyperbolic equations*, Journal of Computational Physics, 490, 2023, 112304.

[31] B. C. Yee, S. S. Oliveira, T. S. Haut, M. Holec, V. Z. Tomov and P. G. Maginot, *A quadratic programming flux correction method for high-order DG discretizations of SN transport*, Journal of Computational Physics, 419, 2020, 109696.

[32] D. Yuan, J. Cheng and C.-W. Shu, *High order positivity-preserving discontinuous Galerkin methods for radiative transfer equations*, SIAM Journal on Scientific Computing, 38(5), 2016, A2987-A3019.

[33] M. Zhang, J. Cheng and J. Qiu, *High order positivity-preserving discontinuous Galerkin schemes for radiative transfer equations on triangular meshes*, Journal of Computational Physics, 397, 2019, 108811.

[34] X. Zhang and C.-W. Shu, *On positivity-preserving high order discontinuous Galerkin schemes for compressible Euler equations on rectangular meshes*, Journal of Computational Physics, 229(23), 2010, 8918-8934.